

LASER INTERFEROMETER GRAVITATIONAL WAVE OBSERVATORY
- LIGO -
CALIFORNIA INSTITUTE OF TECHNOLOGY
MASSACHUSETTS INSTITUTE OF TECHNOLOGY

Document Type	LIGO-P950017-02 -	E	6/24/96
The Laser Interferometer Gravitational- Wave Observatory (LIGO) Project			
Dennis Coyne			

**Amended version of a Publication in the
*Proceedings of the IEEE 1996
Aerospace Applications Conference
4-9 February 1996, Snowmass, CO***

California Institute of Technology
LIGO Project - MS 51-33
Pasadena CA 91125
Phone (818) 395-2129
Fax (818) 304-9834
E-mail: info@ligo.caltech.edu

Massachusetts Institute of Technology
LIGO Project - MS 20B-145
Cambridge, MA 01239
Phone (617) 253-4824
Fax (617) 253-7014
E-mail: info@ligo.mit.edu

WWW: <http://www.ligo.caltech.edu/>

CHANGE RECORD			
REVISION	DATE	PAGES AFFECTED	ITEM(S) AFFECTED
0	12/26/95	Initial Publication	--
1	6/13/96	pg. 10, Table 3	For the initial interferometer, the mirror mass was changed from 12 kg to 11 kg and the mirror diameter was changed from 0.28 m to 0.25 m. The pendulum period was also changed from 1 sec to 0.744 sec.
		pg. 13, Figure 7	Corrected the seismic curve (crossing suspension thermal at ~40 Hz rather than ~100 Hz)
		pg. 17 (and ref. [27] on pg. 31)	Equation for "Residual Gas" phase noise corrected per reference [27b]
		pg. 19	changed "over 140 km of welds" to "approximately 100 km of welds (depending upon beam tube skelp width)"
		pg. 20	changed "worlds's largest high performance vacuum system" to "worlds's largest ultra-high ($<10^{-9}$ torr) vacuum system"
2	6/24/96	pg. 17	Equation for "Residual Gas" phase noise corrected (moved L out from under the square root).

The Laser Interferometer Gravitational-Wave Observatory (LIGO) Project

Dennis C. Coyne
California Institute of Technology
Physics, Math and Astronomy Department
LIGO Project, Mail Code 51-33
Pasadena, CA 91125
818-395-2034
coyne@ligo.caltech.edu

Abstract—Albert Einstein's general theory of relativity (and all other relativistic theories of gravity) predict Gravitational Waves (GW). To date gravitational waves have not been observed directly (unambiguously). The emission mechanisms and interaction phenomena for gravitational waves are very different than for electromagnetic waves. Most GW sources will not be seen electromagnetically and conversely, most electromagnetic sources will not be seen by GW detectors. Astrophysical sources of gravitational waves include coalescing binary compact systems (neutron stars and black holes), supernovae, rotating pulsars and the stochastic background (as a result of the big bang and the gravitational analog to the cosmic microwave background). The Laser Interferometer Gravitational Wave Observatory (LIGO), a National Science Foundation sponsored project being performed jointly by the California Institute of Technology and the Massachusetts Institute of Technology, is one of a new class of astronomical instruments designed to probe the universe by detecting gravitational waves. Signal characteristics and expected event rates for these sources are discussed. A brief history of interferometric gravitational wave detectors and reference to ongoing and collaborative international projects is also provided.

LIGO will consist of two widely separated sites at which L-shaped vacuum systems, each with two 4 km long arms, will house interfer-

ometers for coincident detection of gravitational waves. The initial LIGO detector consists of 3 interferometers, two at one site and one at the other. Each interferometer measures the motion of freely suspended and seismically isolated masses induced by a GW. Correlations among the three interferometers will be used to eliminate events due to terrestrial noise. The LIGO facilities are designed to be extensible with the intent to add and upgrade interferometers in the future.

Each initial LIGO interferometer is fundamentally a Michelson interferometer with resonant cavities in each arm designed to detect differential motion at acoustic frequencies (100 Hz - > 3 KHz) between its arms as small as 10^{-18} m rms. The basic strategy for detecting the minute GW effect is (i) use of a very long baseline (4 km), (ii) high laser power (≥ 6 W at the interferometer input and > 8 kW resonant in the arms), (iii) long effective arm lengths (with light storage times of about 1 ms), (iv) geographically isolated and seismically quiet sites (Hanford, WA and Livingston, LA), (v) cascaded, multi-stage seismic isolation systems and pendulum suspensions for the test masses ($\sim 10^{-12}$ transmission of ground motion at 100 Hz) and (vi) massive, suspended, high-Q test masses (to reduce thermal noise contributions).

Partially transmitting mirrors in each arm form resonant (Fabry-Perot) cavities with the end

mirrors in order to increase the effective arm length (and strain sensitivity) and increase the power. The two optics which form the Fabry-Perot resonant cavities are the suspended "test" masses used to sense the gravitational waves. An incident GW will cause differential changes in the length of the two arms of the interferometer; The difference in length will depend on angle of incidence and polarization of the wave. Length change is sensed by a photodetector (operating at a dark fringe of the interference field) from which the effect of a passing gravitational wave is inferred. A laser beam is used as a single-frequency, single-mode light source. Its frequency is servo-locked to the average length of the arms of the interferometer. The principles of operation of the initial LIGO detector system are discussed.

A sensitivity of $\sim 5 \times 10^{-19} \text{ m}/\sqrt{\text{Hz}}$ ($\sim 1 \times 10^{-20}/\sqrt{\text{Hz}}$ strain) has been demonstrated in a 40 m prototype detector at the California Institute of Technology over a measurement band of 250 Hz to 1.5 kHz, which is close to the initial LIGO target displacement sensitivity curve (minimum sensitivity of $\sim 1 \times 10^{-19} \text{ m}/\sqrt{\text{Hz}}$ at $\sim 200 \text{ Hz}$). For future advanced interferometers, achieving a sensitivity goal of $10^{-24}/\sqrt{\text{Hz}}$ strain corresponding to an optical phase shift sensitivity of $10^{-11} \text{ rad}/\sqrt{\text{Hz}}$ over a measurement band of 10 Hz to 10 kHz (which will yield high event rates for coalescing binary gravitational wave sources) will require a thorough understanding of the limitations of detection due to a number of noise sources, including seismic, thermal, shot, stray light, and gravity gradients. The fundamental limiting noise sources are quantitatively described.

Key design implementation considerations for the facilities and design aspects of the detector such as high performance optical baffling, high reflectivity (1 ppm loss) and optically flat ($\lambda/600$ rms) surfaces on high mechanical Q mirror substrates (Qs on the order of 10^7) are also

described. The future of gravitational wave detectors and some concepts for advanced optical detectors are briefly described.

TABLE OF CONTENTS

1. INTRODUCTION
2. BACKGROUND & HISTORY
3. ASTROPHYSICAL INTEREST
4. PRINCIPLES OF OPERATION
5. LIMITS TO PERFORMANCE
6. IMPLEMENTATION/DESIGN
8. CONCLUSIONS

1. INTRODUCTION

The Laser Interferometer Gravitational Wave Observatory (LIGO), a National Science Foundation sponsored project being performed jointly by the California Institute of Technology and the Massachusetts Institute of Technology, is one of a new class of astronomical instruments designed to probe the universe by detecting gravitational waves [1]. Sources of interest include coalescing binary compact systems (neutron stars and black holes), supernovae, rotating pulsars and the stochastic background (as a result of the big bang and the gravitational analog to the cosmic microwave background).

LIGO comprises two remotely located observatory sites (Figure 1) where the detector system(s) and all support facilities are located and also includes laboratories, prototype interferometer facilities, research and development, and design facilities at the associated Universities.

The initial detector will consist of three independent laser interferometers operating in coincidence or correlation. Interferometers will be built on two scales, two interferometers will have arm lengths of 4 km and the third will have arm lengths of 2 km. The lengths are constrained by considerations of site topogra-

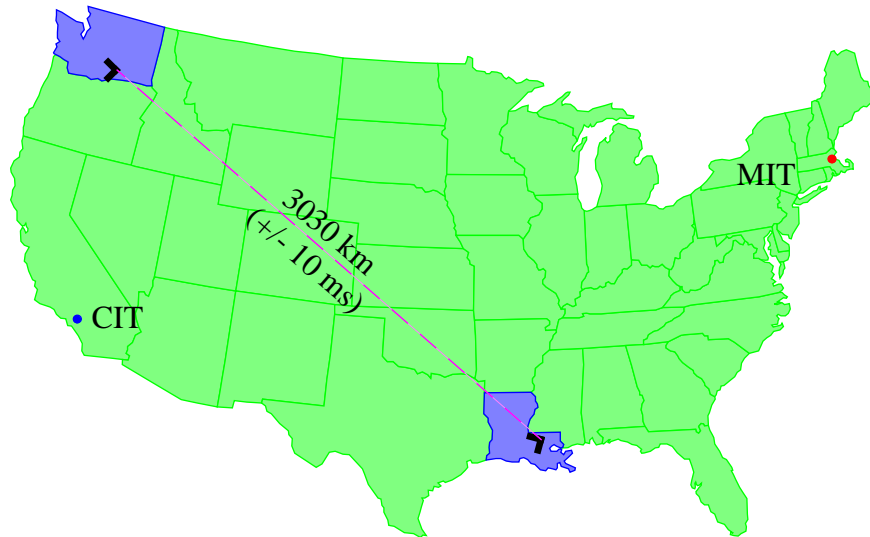


Figure 1: LIGO Sites

phy and associated costs of additional earth removal. Each interferometer is in a Michelson ("L") configuration with resonant Fabry-Perot cavities in the arms.

The two LIGO observatory sites selected are (i) at the DOE Hanford Nuclear Facility in Washington State (denoted "Hanford"), and (ii) in Livingston Parish, Louisiana (denoted "Livingston"). The Hanford site will house two instruments in the same vacuum envelope: a full length (4 km) and the half length (2 km) interferometer. The site at Livingston will contain a single 4 km interferometer. The vertex of the Hanford instrument is at geographic coordinates $46^{\circ} 27' 18.5''$ N, $119^{\circ} 24' 27.1''$ W, with arms oriented toward the northwest at a bearing $N36.8^{\circ} W$ and the southwest at a bearing $S53.2^{\circ} W$. The vertex of the Livingston Louisiana site is at geographic coordinates $30^{\circ} 33' 46.0''$ N, $90^{\circ} 46' 27.3''$ W, with arms oriented southeast at a bearing $S18^{\circ} E$, and southwest at a bearing $S72^{\circ} W$. The separation of the sites is 3030 km which corresponds to a maximum time-of-arrival difference for gravitational waves at the two sites of approximately ± 10 ms (i.e. the separation distance divided by the speed of a GW, which

must equal the speed of light if, as theory predicts, the graviton has zero rest mass). The interferometer arms at the two sites are oriented for maximum coincidence sensitivity for a single gravitational wave polarization. This is achieved by having one arm of each interferometer oriented at the same angle relative to the great circle passing through the two interferometer vertices. The two arms of each interferometer are perpendicular and lie very close to the local horizontal plane at the intersection of the arms.

The data from the detector will be analyzed for burst, chirped, periodic signals as well as for stochastic background gravitational waves (i.e. the GW analog to the cosmic microwave background radiation). Accurate and precise absolute timing shall be provided by the Global Positioning System (GPS). This will permit operating with narrow coincidence gates among the interferometers and also permits correlation of LIGO data with other detector systems, such as resonant bar detectors, particle (neutrino) detectors, and electromagnetic (γ -ray, x-ray, visible, infrared, and radio) astronomical observatories. The two sites have been chosen to be sufficiently separated so that environmental perturbations to the interferom-

eters are expected to be independent and hence uncorrelated. The gravitational waves signals will be correlated and this property is used in making the observation. At both sites an environment monitoring system is used to measure the environmental perturbation to the interferometers to reduce the singles rate in a burst search, to measure the background perturbations that could influence a periodic and stochastic gravitational wave measurement, and as a diagnostic for interferometer development. In addition, all relevant interferometer and system parameters that can potentially affect the noise budget shall be recorded for subsequent diagnostic studies.

The operation of a half length and a full length interferometer at one site serves several functions: it improves the rejection of accidental coincidences by imposing a triple coincidence for a valid burst event, is a diagnostic for gravitational waves by demanding that a true signal be in the ratio of the interferometer lengths and finally enables a broad-band search for a stochastic gravitational wave background limited by the environmental correlations at a single site.

The LIGO detector has the capability of making a confident detection of gravitational waves alone. To obtain the maximum scientific return, LIGO is also planned to be operated as an element of an international network of gravitational wave detectors involving other long baseline interferometric detectors and acoustic detectors. Long baseline interferometric detectors are expected to be in operation by the VIRGO Project at Pisa, Italy and the GEO600 project at Hannover, Germany. Plans are also underway to establish long baseline interferometric detectors in Japan and Australia. A global network of detectors (Table 1) will be able to provide full information from the gravitational waves, in particular, the wave polarization and the source position on the sky. Simultaneous observations in several systems

also improves the confidence of a detection. Acoustic detectors that are expected to be operating at the inception of the LIGO are in: Frascati, Italy; Baton Rouge, Louisiana; and Perth, Australia.

Table 1: International Gravitational Wave Interferometer Projects

Project	Country	Number	Length (km)
LIGO	United States	2	4.0
		1	2.0
VIRGO	Italy & France	1	3.0
GEO600	Germany & Britain	1	0.6
TAMA	Japan	1	0.3
AIGO	Australia	1	1.0

2. BACKGROUND & HISTORY

The idea to use optical (laser) beam detectors for GW detection was first suggested in 1956 by Pirani at the Imperial College. Gertsenshtein and Pustovit explicitly suggested use of an optical interferometer for GW detection in 1962. Then in the mid-1960s J. Weber independently discovered the idea but did not publish or pursue it.

The concept was independently re-discovered by R. Weiss at MIT in 1970. Weiss carried out detailed design and feasibility studies in 1971-72. R. Forward of Hughes Corp. constructed the first working prototype and achieved a strain sensitivity of $2 \times 10^{-16} 1/\sqrt{Hz}$. (Required strain levels are discussed in the next section.) This work languished due to lack of further funding. In the mid-1970s, The Mach Planck Institute at Garching pursued Weiss' design (a Michelson interferometer with arm delay lines).

Concurrently, R. Drever conceived of the idea of an arm resonant (Fabry-Perot) cavity inter-

ferometer (the LIGO baseline design) at Glasgow University. In 1979, Drever moved to Caltech to pursue large-scale prototype research and initiated the development of the LIGO 40 m prototype interferometer. In 1983, A. Brillet initiated an interferometer design at Orsay, France which eventually lead to the ongoing VIRGO project, a joint French-Italian venture. In 1985 through 1989, a collaboration between Caltech and MIT, promoted by the NSF, developed the basis for the current LIGO project. More detailed background and history on GW detection can be found in references [2], [3], [4], [5] and [6].

3. ASTROPHYSICAL INTEREST

The motivation for performing gravitational wave astrophysical observation stems from the significant differences between electromagnetic waves and gravitational waves, the need for experimental confirmation of the existence of gravitational waves and the desire to explore GW sources.

The observations carried out by the LIGO are expected to provide fundamental and new information concerning the gravitational interaction including:

- direct measurement of strong field gravity through the observation of the gravitational waves from black holes. The waves will convey information about
 - the normal modes of black holes
 - inertial frame dragging by rotating black holes
- through the observation of compact stellar systems such as neutron star/neutron star, black hole/black hole and black hole/neutron star binaries provide detailed information of the relativistic equations of motion.
- the direct measurement of the polarization states of gravitational waves (possible in conjunction with other interferometric gravitational wave detectors).
- a direct measurement of the speed of prop-

agation of gravitational waves.

The astrophysical information derived from LIGO observations includes:

- the spatial and mass distribution of neutron star binary systems in the universe.
- the spatial and mass distribution of black holes and black hole binary systems in the universe.
- a new and independent method of determining the Hubble expansion using compact binary systems as standard objects.
- the equation of state of neutron stars from the gravitational waveforms at the final coalescence of neutron star binaries.
- the internal dynamics of asymmetric supernova explosions.
- limits to or measurements of the gravitational multipole moments of pulsars.
- limits or observations of the gravitational wave background from the earliest epoch of cosmic evolution.
- a new view of the universe with a high probability of uncovering phenomena not observed by electromagnetic astronomy.

A propagating GW (a spacetime distortion) produces time-dependent body forces [7]. The effect upon a body at rest (if it could be measured) is a cyclical elongation and contraction, as indicated in Figure 2. Unlike the electromagnetic wave, the GW is a tensor wave. However, the time (t) dependent propagation in free space (coordinate vector, r) is just like an electromagnetic wave (with the exception that there is negligible absorption, scattering or dispersion) and is given by:

$$h(t, \hat{r}) = h e^{i(\hat{k} \cdot \hat{r} - \omega t)}$$

where \hat{k} is the wave vector and denotes the direction of propagation, ω is the temporal frequency and h is the GW induced strain, analogous to the electric field strength, E. Like E, h can be decomposed into two orthogonal polarizations, h_x and h_+ .

Gravitational waves are the result of oscillations of second and higher order multipole moments of mass and mass “current”, whereas electromagnetic waves are the result of oscillations of first and higher order electric and magnetic multipole moments. The dominant

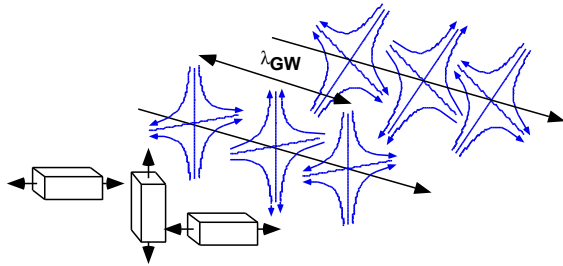


Figure 2: Passage of a GW (x and + polarizations) distorts spacetime and produces time-dependent body-forces

moment for GW emission is the mass quadrupole, $M_2 \sim Mr^2$, where M is the source’s total mass and r is the average lengthscale of its deviations from spherical symmetry. The contributions to the two polarizations of the GW due to the quadrupole moment are:

$$h_x \sim h_+ \sim \left(\frac{G}{c^4 r}\right) \frac{d^2 M_2}{dt^2}$$

where h is the strain amplitude. For compact relativistic sources, the second derivative of the quadrupole mass moment can be approximated by Mv^2 (where v is the average internal velocity of the source) which is equal to the kinetic energy associated with internal, non-spherical motions of the source, $E_{kinetic}^{ns}$. Consequently, the amplitude of the oscillations of the GW components, h_x and h_+ , can be expressed as:

$$h \sim \left(\frac{GE_{kinetic}^{ns}}{c^4 r}\right) \sim 10^{-20} \left(\frac{E_{kinetic}^{ns}}{M_{sun} c^2}\right) \left(\frac{10Mpc}{r}\right)$$

where M_{sun} is the solar mass and 10 megapar-

secs (Mpc), or 30 million light years, is the distance to the Virgo cluster of galaxies (the nearest large cluster of galaxies to our own Milky Way galaxy). The strongest astrophysical sources are likely to have masses on the order of our sun, or even a few factors of ten larger, internal velocities between 0.1 c and c where c is the speed of light, and will be located (at the closest) at roughly the distance to the center of the Virgo cluster. Consequently, the strongest GW waves arriving at the Earth will have upper limits to their amplitudes h of $\sim 10^{-20}$, and will likely be much smaller (10^{-22} or so). However, “local” (within our own galaxy) cataclysmic events although exceedingly rare (visible supernovae in our own galaxy occur at a rate of 3-4/century and the actual rate is believed to be ~ 10 times higher), will have much greater strength. It is estimated that the supernova in 1987 would have produced a burst signal-to-noise ratio (SNR) of 100 in LIGO.

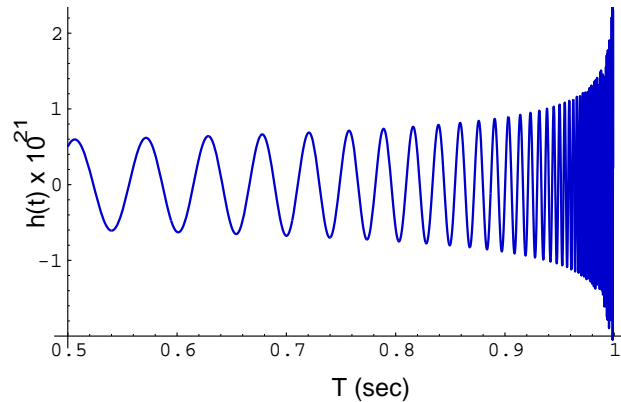


Figure 3: “Chirped” Strain Signal Produced by a Binary Neutron Star Inspiral

An example of the expected signals is the “chirped” signal produced by the inspiral of a binary neutron star system just before the two bodies coalesce (Figure 3). The strain amplitude induced by this type of source varies as follows:

$$h \sim (t_{\text{coalescence}} - t)^{-\frac{1}{4}}$$

and the frequency varies as:

$$f \sim (t_{\text{coalescence}} - t)^{-\frac{3}{8}}$$

The total duration of an event which is detectable by LIGO will be seconds.

The expectation of detectability of gravitational-wave sources by LIGO is based primarily upon the best understood (theoretically) of candidate sources, the final, minute-long inspiral of a neutron star binary. At LIGO's lowest detection frequency, the ~10 km sized stars are ~100 km apart and not yet tidally disrupting each other, so that their wave emission is well understood [8], [9], [10], [11]. The uncertainty in the wave amplitude reflects the uncertainty regarding the distance to the nearest such sources. Best estimates, based on extrapolations of the statistics of neutron stars in our galaxy, give 200 Mpc (650 million light years) for the distance to which LIGO must look to see three neutron inspirals per year. Analysis of the uncertainties in this data give an "ultraconservative upper limit" of 1000 Mpc and an "optimistic lower limit" of 23 Mpc.

The performance of the interferometer is characterized by its strain sensitivity spectrum, $\tilde{h}(f)$, or noise floor, in units of $1/\sqrt{\text{Hz}}$. The signal-to-noise-ratio (SNR) for measurement of a GW burst [1] (such as from an inspiraling black hole binary) with an amplitude of h_{amp} , a characteristic (mean) frequency f_c and duration

$$\text{of } n \text{ cycles, is: } SNR = \frac{h_c}{h_{\text{rms}}} = \frac{h_{\text{amp}}\sqrt{n}}{\sqrt{f_c}\tilde{h}(f_c)}$$

where h_c is referred to as the wave's characteristic amplitude and h_{rms} is the interferometer's root mean square (rms) noise for a one-cycle long burst at the source's characteristic fre-

quency.

A comparison of expected sources (h_c) with the expected performance (h_{rms}) of initial and advanced LIGO interferometers is given in Figure 4. The GWs sweep with time from low frequency to high frequency. As indicated in Figure 3, the amplitude of the GW increases with time. However, the number of cycles spent near each frequency decreases faster than the amplitude. As a consequence, the characteristic amplitude (which determines the signal-to-noise ratio) decreases slightly, as shown in Figure 4. (The vertical arrows along the bottom inspiral source curve mark the remaining time to collision and the distances between the stars.)

The lower curve of each pair in Figure 4 is the rms noise h_{rms} in each 4 km interferometer for a one-cycle burst at the source's characteristic (mean) frequency. The upper curve in each pair is the sensitivity to bursts [1], $h_{SB} = 11h_{\text{rms}}$, i.e. the strength h_c that a burst must have — if it arrives only rarely, from a random direction, with a random polarization and at a random, unpredictable time — in order to be highly confident that it is not due to Gaussian noise. (If the neutron star collision can be independently observed, e.g. via a gamma ray detector, then the waves can be identified with confidence at $h_c = h_{SB}/3$, or a factor of 3 below the upper curves in Figure 4.) Based upon the comparison in Figure 4, one concludes that the initial LIGO detectors might be capable of detecting 3 events/yr. at the optimistic level and advanced interferometers will be capable of performing comparably at the "ultraconservative" level.

4. PRINCIPLES OF OPERATION

Each initial LIGO interferometer is fundamentally a Michelson interferometer designed to detect differential motion between its arms as

small as 10^{-18} m rms. The basic strategy for detecting the minute GW effect is:

- (1) use of a very long baseline (4 km)
- (2) high laser power (≥ 6 W at the interferometer input and > 8 kW resonant in the arms)
- (3) long effective arm lengths (with light storage times of about 1 ms)
- (4) isolated seismically quiet sites (Hanford, WA and Livingston, LA)
- (5) cascaded, multi-stage seismic isolation systems and pendulum suspensions for the test masses ($\sim 10^{-12}$ transmission at 100 Hz) and

(6) massive, suspended, high-Q test masses (to reduce thermal noise contributions).

The measurement goal of 10^{-18} m rms (or 10^{-12} of a wavelength of visible light) requires a phase shift measurement of 10^{-9} rad rms (as shown in the next section). Since the phase measurement shot noise limit (also discussed

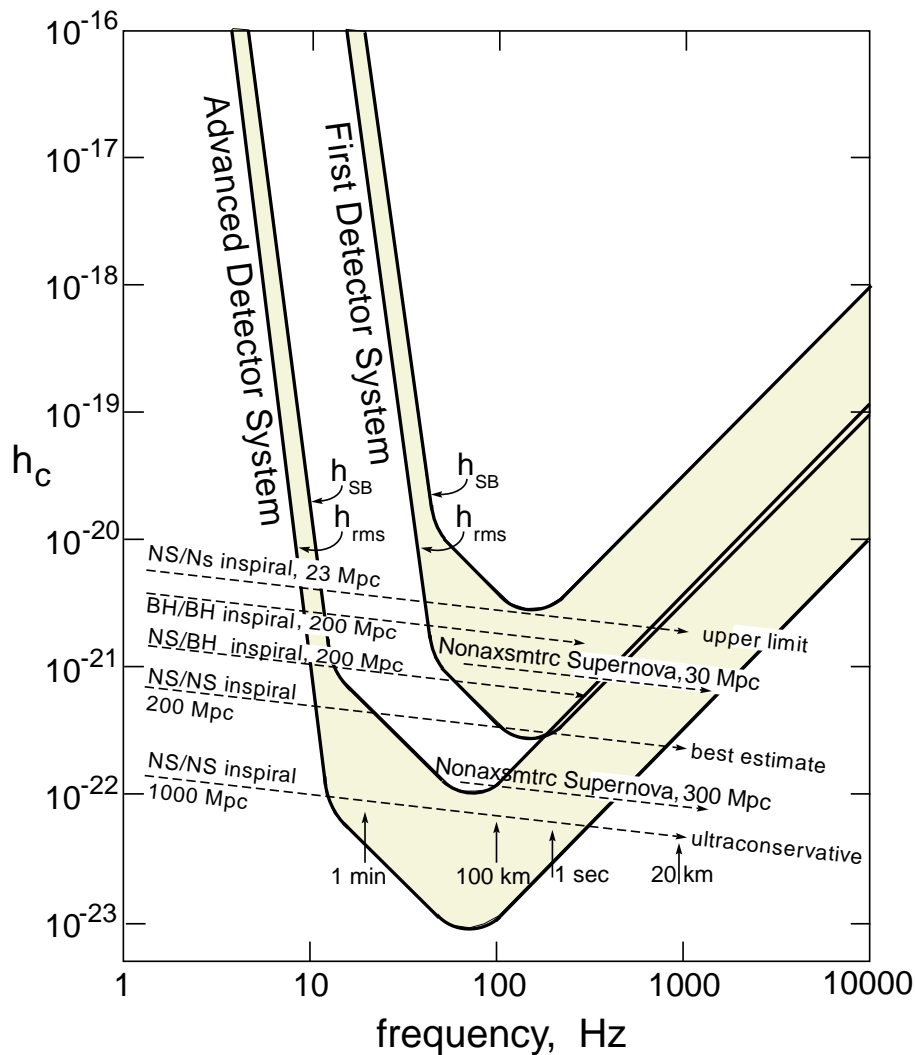


Figure 4: Comparison of LIGO sensitivities and Estimated Wave Strengths
 Expected rms noise h_{rms} in LIGO's initial and advanced detector systems and the characteristic amplitude h_c of gravitational wave bursts from several hypothesized sources. (NS = neutron star, BH = black hole)

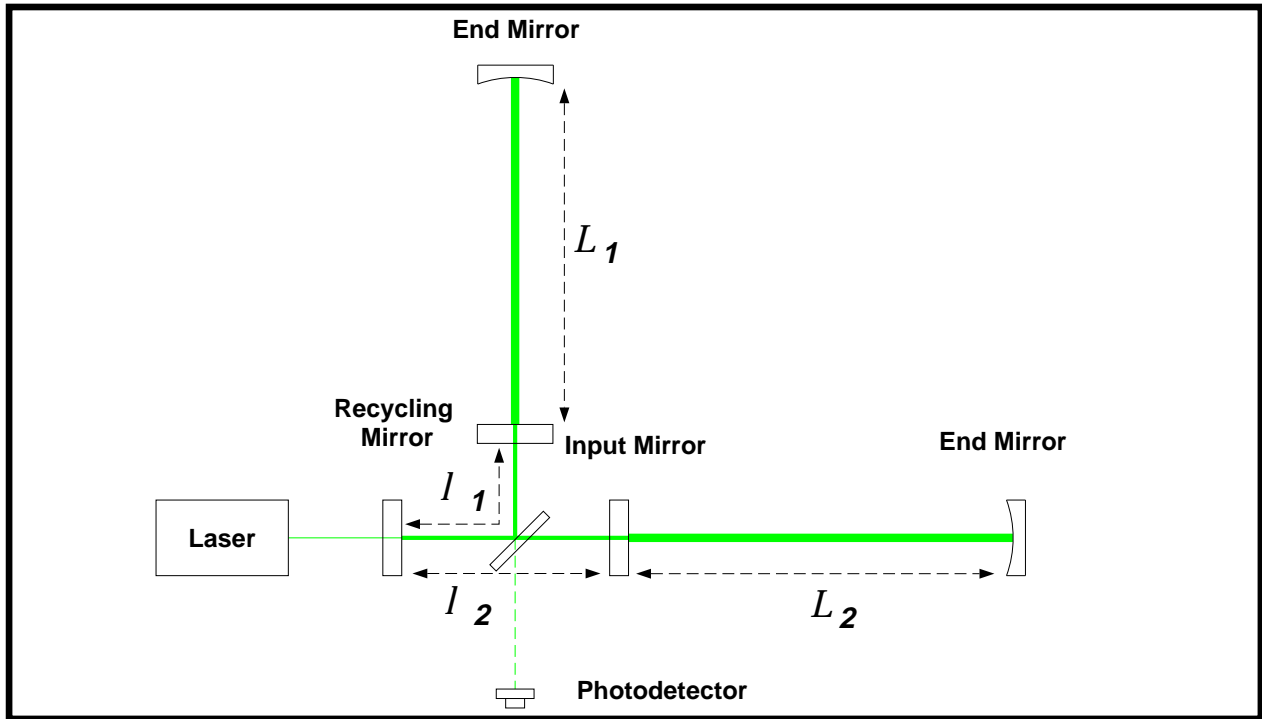


Figure 5: Basic Configuration

in the next section) varies inversely with the square root of the number of photons in the measurement “period” (0.01 sec for a 100 Hz lower measurement band frequency) 10^{18} photons are required in 0.01 sec. This corresponds to about 20 W of power (at 1.064 microns). The amplitude of vibrational motion of the atoms in the mirrors exceeds the GW signal but occurs at a frequency of $\sim 10^{13}$ Hz, far above LIGO’s GW band (~ 3 kHz). However, thermal excitation does excite the normal modes of the mirrors at frequencies of ~ 20 kHz with amplitudes on the order of 10^{-16} m. The interferometer averages this effect over many periods and is sensitive only to the changes of amplitude, which are made small by giving the mirrors high mechanical Qs.

Two methods are employed to increase the light power used to sense the motion of the test mass mirrors (and thereby decrease the effect of shot noise). The first method is to incorporate resonant (Fabry-Perot) cavities

in the Michelson arms [12]. The second method is to “recycle” the light from the bright fringe output port of the Michelson (i.e. light going back from the interferometer toward the laser) by reflecting it back into the interferometer [12], [13]. This arrangement, called a power recycling interferometer, can result in an additional gain of about 30 in power.

All the optical components in the phase sensitive part of the interferometer are suspended as pendula to reduce the coupling to seismic and thermal noise and to provide a means to control the optical path lengths in the interferometer. A highly stabilized laser beam is injected into the two arms of the interferometer via a beamsplitter and servo-locked to the average length of the arms of the interferometer. The path lengths are maintained by servo systems to hold the light incident on the detector, placed at the antisymmetric port of the beam splitter, at a dark fringe.

A GW incident normal to the plane of the interferometer and appropriately polarized, disturbs this condition by inducing an antisymmetric path

length change ($L_1 - L_2$ in Figure 5) in the two orthogonal Fabry - Perot cavities thereby increasing the intensity at the photodetector. When the interferometer is operated in this manner, the light not absorbed or scattered by the optical components is reflected by the interferometer and returned to the laser at the symmetric port of the beam splitter. In the initial LIGO detector a mirror is placed between the laser and the interferometer to enclose the entire interferometer into an optical cavity.

Table 2: LIGO Interferometer Optical Parameters

OPTICAL CHARACTERISTICS	NOMINAL INITIAL INTERFEROMETER	SAMPLE ENHANCED INTERFEROMETER
Arm Length	4000 m	4000 m
Laser Type & Wavelength	Nd:YAG, $\lambda = 1.064 \mu\text{m}$	Nd:YAG, $\lambda = 1.064 \mu\text{m}$
Input Power, P	6W	100W
Contrast Defect, I-c	3×10^{-4}	3×10^{-4}
Mirror Loss, L_M	1×10^{-4}	1.3×10^{-5}
Power Recycling Gain	30	380
Arm Cavity Storage Time, τ_{Arm}	8.8×10^{-4} s	1.3×10^{-3} s
Cavity Input Mirror Transmission, T	3×10^{-2}	2×10^{-2}
Total System Loss, $L_T = (T+A + \text{Scattering})$	4×10^{-2}	3×10^{-3}

Table 3: LIGO Interferometer Mechanical Parameters

MECHANICAL CHARACTERISTICS	NOMINAL INITIAL INTERFEROMETER	SAMPLE ENHANCED INTERFEROMETER
Mirror Mass, M_M	11 kg	40 kg
Mirror Diameter, D_M	.25 m	.40 m
Mirror Internal Q_M	1×10^6	3×10^7
Pendulum Q_P (damping mechanism)	1×10^7 (material)	1×10^8 (material)
Pendulum Period, T_P	0.74 s (Single)	1 s (Double)
Seismic Isolation System	T(100 Hz) = -100 dB	T(10 Hz) = -100 dB

The position and reflectivity of this mirror is chosen so that the light from the laser is added constructively with that circulating in the interferometer while the light reflected by the mirror back to the laser is combined destructively with the light transmitted by this mirror from the interferometer. The net result is that little light is returned to the laser and the optical power circulating in the interferometer is increased by the reciprocal of the interferome-

ter optical loss. The increase in sensitivity to length changes is equivalent to using a more powerful laser source.

Figure 5 shows a schematic of the initial interferometer configuration. Tables 2 and 3 present the design parameters of the presently planned (initial) interferometers. Also presented in the tables are sample parameters for contemplated enhanced interferometers. In later phases of the LIGO more radical changes in the interferometer configurations are expected such as signal recycled, resonant and frequency agile systems leading to advanced detectors.

A Michelson interferometer is chosen as the basic topology since the sensitivity of its differential length measurement to the laser frequency stability can be made small. Phase instability of the laser results in displacement noise in an interferometer with unequal path lengths. An analysis [14] of the spectral power distribution in the output of a Michelson interferometer illuminated by a light source with a Gaussian temporal distribution of phase noise, indicates that the displacement squared per unit frequency in the interferometer is given by [15]:

$$\frac{\Delta x^2(f)}{\Delta f} = \frac{4}{3} \lambda^2 \delta^2 \tau^3$$

for the case $f\tau \ll 1$ and $\delta\tau \ll 1$, where τ is the difference in light transit time between the two paths in the interferometer, λ is the laser wavelength and δ is the oscillating frequency width of the laser. The difference in light travel time, τ , can be made arbitrarily small in the Michelson, so that excessive demands are not made on the stability of the laser, δ . In a typical case, δ might be on the order of 10 Hz and τ approximately 10^{-9} sec, which gives

$$h = \frac{\Delta x}{L\sqrt{\Delta f}} \sim 10^{-22} (1/\sqrt{Hz})$$

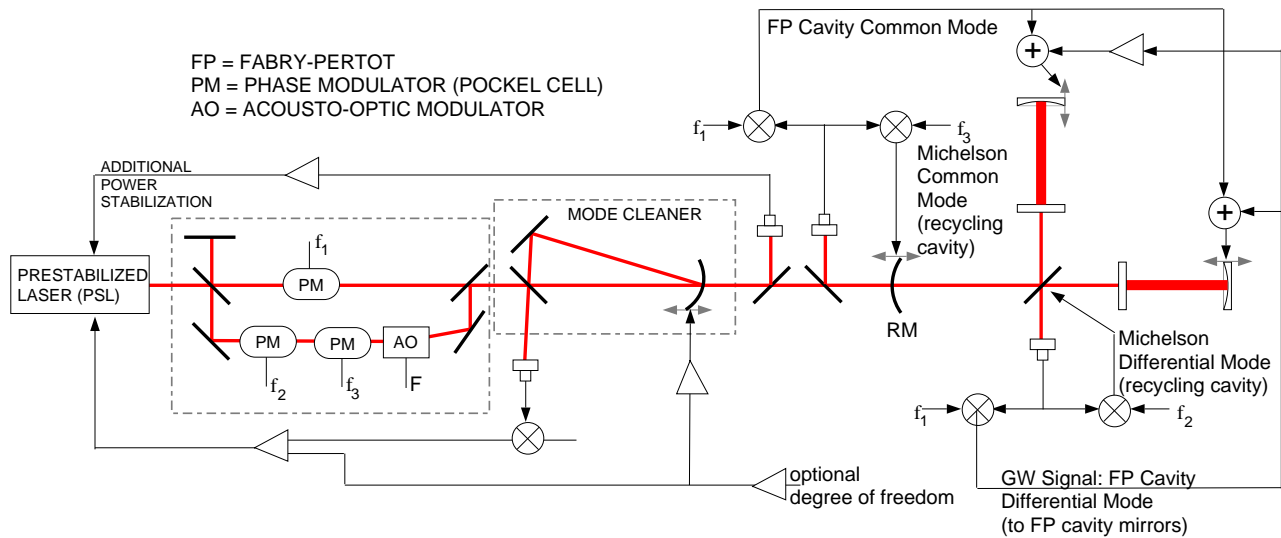


Figure 6: Modulation and Length Sensing/Control Servo-System Topology

The arms of the interferometer, and the finesse (“bounce” factor) of the Fabry-Perot cavities can be made as large as is consistent with the condition that the storage time of the light is less than one-half the period of the gravitational wave that is to be detected.

The interferometer is held on a fixed fringe by a servo system which maintains the optical delay in both arms; the output signal of the servo system is proportional to the differential strain in the two arms induced by the gravitational wave.

In the basic optical topology of Figure 5, four resonant conditions are required for operation corresponding to four degrees of freedom:

- differential motion of the cavities (the gravitational wave signal, or L_1-L_2)
- common mode motion of the cavities (L_1+L_2)
- differential motion of the Michelson arms formed by reflection off of the near sides of the corner test mass mirrors (l_1-l_2)
- common mode motion of the Michelson arms (l_1+l_2)

It is possible to replace one of these servo controlled lengths with feedback control of the laser wavelength (frequency). The servo sys-

tem signals are derived from the photodetector by synchronous detection at the modulation frequency.

In order to mitigate the effects of laser amplitude fluctuations (above shot noise), a modulation scheme is employed to shift the measurement to a higher frequency [15] (about 10 MHz). The basic modulation carrier frequency of the beam is accomplished through the use of electro-optical phase modulating crystals (Pockel-effect phase shifters).

Several methods for phase detection using modulated light and several control topologies [16],[17] have been, and continue to be, explored for use on the full-scale LIGO system. The frequency-shifted subcarrier approach [18] depicted in Figure 6, is a leading candidate for implementation in LIGO. To sense the lengths, phase modulation is applied to the input light. The laser single line frequency is the carrier frequency; All other frequencies are generated by impressing sidebands on the carrier. The frequencies used, the sensed location and the degrees of freedom to which they are sensitive are listed in Table 4.

Length change measurement is accomplished

via the reflection locking technique [19]. Maximum sensitivity to a sensed degree of freedom is achieved when the sideband field is independent of the sensed degree of freedom, so that it acts as a constant reference for interference with the carrier. The carrier is selected to be resonant in a sensed cavity and the sidebands are chosen to be sufficiently outside the cavity resonance, so that only the carrier is sensitive to changes in cavity length.

Table 4: Signals sensitive to length degrees of freedom

INTERFERING FIELDS	SIGNAL LOCATION	DEGREE OF FREEDOM
C and CSB	anti-symmetric port	L_1-L_2 , differential arm cavity length
C and CSB	reflected from recycling mirror	L_1+L_2 , common mode arm cavity length
FSSC and SCSB1	anti-symmetric port	l_1-l_2 , differential mode Michelson length
FSSC and SCSB2	reflected from recycling mirror	l_1+l_2 , common mode Michelson length

The modulation frequencies in the frequency-shifted subcarrier approach are chosen so that:

- all frequencies that propagate in the interferometer are resonant in the recycling cavity for coupling efficiency (i.e. all frequencies except SCSB2);
- the carrier (C) and carrier-sideband (CSB) family is used for arm cavity (Fabry-Perot) length sensing, so C is resonant in the Fabry-Perot cavities, while the CSB is not;
- the frequency-shifted, subcarrier (FSSC) and its first sideband (FSSB1) are used to sense the recycling cavity length, and are selected to be anti-resonant in the Fabry-Perot cavities to ensure insensitivity to arm

cavity length; and

- the second set of sidebands on the frequency-shifted subcarrier (FSSB2) do not couple into the interferometer at all, so they are chosen to have minimal overlap with recycling cavity modes to ensure low coupling to the interferometer

Optimization of the interferometer configuration involves a detailed, coupled many-dimensional study including five mirror radii of curvature and mirror reflectivities, four lengths, and three families of frequency modulated light and their relative frequency shifts. Selection of each of these parameters can impact the choice of another parameter and, in general these parameters are subject to constraints (physical, technical or performance related). Studies and experiments to refine the LIGO configuration are on-going.

5. LIMITS TO PERFORMANCE

A thorough understanding of the limitations of detection due to a number of noise sources, including seismic, thermal, shot, stray light, and gravity gradients, is required. The fundamental limiting noise sources are quantitatively described below. First, however, the transfer function of a Fabry-Perot interferometer is discussed. All cases in which strain amplitudes are given, are for the 4 km baseline system. The ensemble of all of the sources of noise are given in the spectral density plots in Figures 7 and 8 for the initial and the example enhanced interferometers, respectively. The limiting noise floor envelope is the root-sum-square (rss) of all effects.

Gravitational Wave Transfer Function

The differential time delay, Δt , in light transiting the two evacuated arms of a single-pass Michelson interferometer corresponds to a measurable optical phase shift:

$$\Delta\phi = \omega\Delta t = \frac{2\pi c\Delta t}{\lambda} = \frac{2\pi\Delta L}{\lambda} = \frac{2\pi hL}{\lambda}$$

If the time light spends in the path (the cavity storage time) exceeds the gravitational wave period (due to a high cavity finesse), signal strength is reduced; this low pass filter behavior of the interferometer limits the high frequency sensitivity:

$$\frac{h(f)}{\phi(f)} \approx \left(\frac{\lambda}{4\pi BL} \right) \sqrt{1 + \left(\frac{2\pi f BL}{c} \right)^2}$$

which is the transfer function from an optical phase shift, ϕ , at the output (antisymmetric port) to the strain amplitude, h , of a gravitational wave which causes the phase shift (at low frequency, $f < c/(4\pi L)$ and for optimal source direction and polarization). In the above expression, the parameter B , the “bounce factor”, is the effective number of bounces made by light in the resonant Fabry-

Perot cavities and is completely analogous to the number of bounces in a delay line interferometer. (B is also related to the finesse or Q of the cavity). The bounce factor can be shown to be $B = 4/T$, where T is the power transmission of the cavity input mirror. From the transfer function it is evident that there is a pole at

$$f = f_o \equiv \frac{c}{2\pi BL} = \frac{1}{4\pi\tau_s}$$

where τ_s is the cavity storage time. Given the system parameters in Table 2, the light storage time (in the Fabry-Perot cavities) is ~ 1 ms, the cavity pole is ~ 80 Hz, and the light phase shift associated with the measurement goal of 10^{-18} m is 10^{-9} rad/s at low frequency. The com-

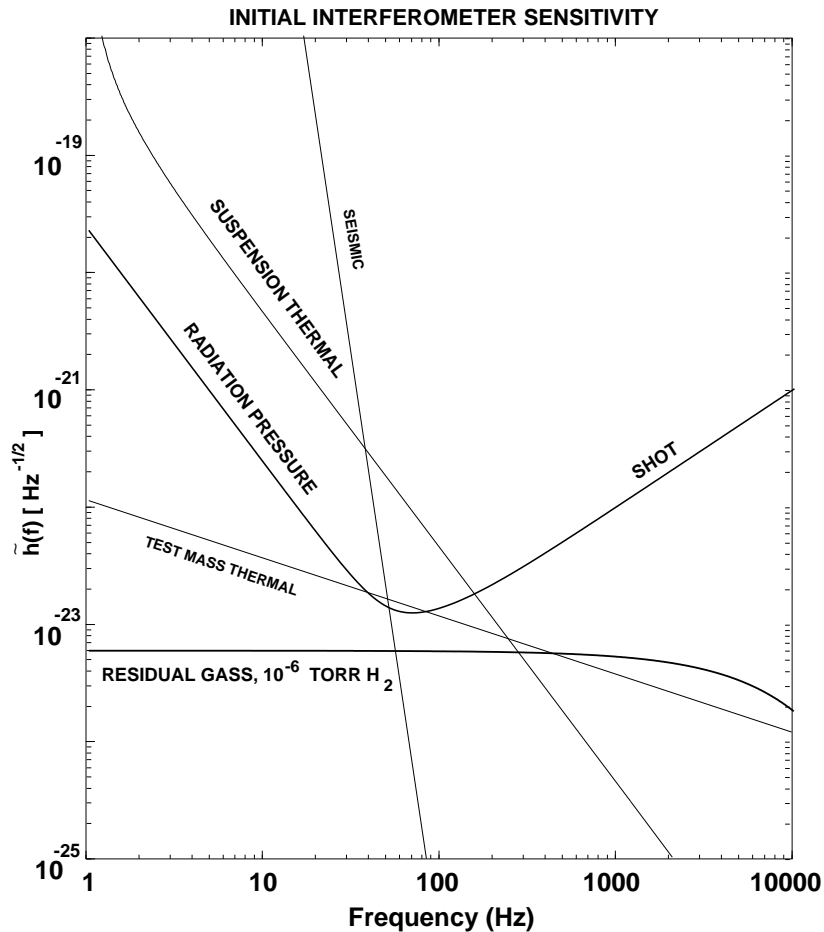


Figure 7: Initial Interferometer Sensitivity

plete transfer function including source angular dependence and polarization can be found in reference [20].

Photon Shot Noise

The detection is dominated by photon counting statistics (shot noise) at high frequencies. The spectral density of the optical phase amplitude resulting from the fluctuating detector current, on the assumption of Poisson statistics (appropriate for light in the coherent state of a single-mode laser) at the antisymmetric port (the photodetector port shown in Figure 5) of the interferometer is given by:

$$\phi_{sn}(f) = \left(\frac{2hc}{\lambda \eta \epsilon P (1 - L_{opt}) G_R} \right)^{1/2}$$

where η = detector quantum efficiency, ϵ =

optical efficiency of the entire optical train, P = laser power, L_{opt} = total optical loss, G_R = broad-band recycling power gain $< 1/L_{opt}$ ($G_R = 1$ for no recycling), λ = optical wavelength, and h = Planck's constant. Basically,

$$\phi_{sn}(f) \sim \left(\frac{hc}{\lambda P} \right)^{1/2},$$

or $\phi_{sn}(f) \sim 10^{-11} \text{ rad}/\sqrt{\text{Hz}}$ for $\lambda = 1.064$ microns and $P = 1.8 \text{ kW}$. Using the DC component of the (optical phase)/(GW strain) transfer function given above, the corresponding shot noise equivalent strain is found to be

$$h_{sn}(f \ll f_o) \approx \phi_{sn}(f \ll f_o) \left(\frac{\lambda}{2\pi BL} \right)$$

using $B = 50$, appropriate for advanced inter-

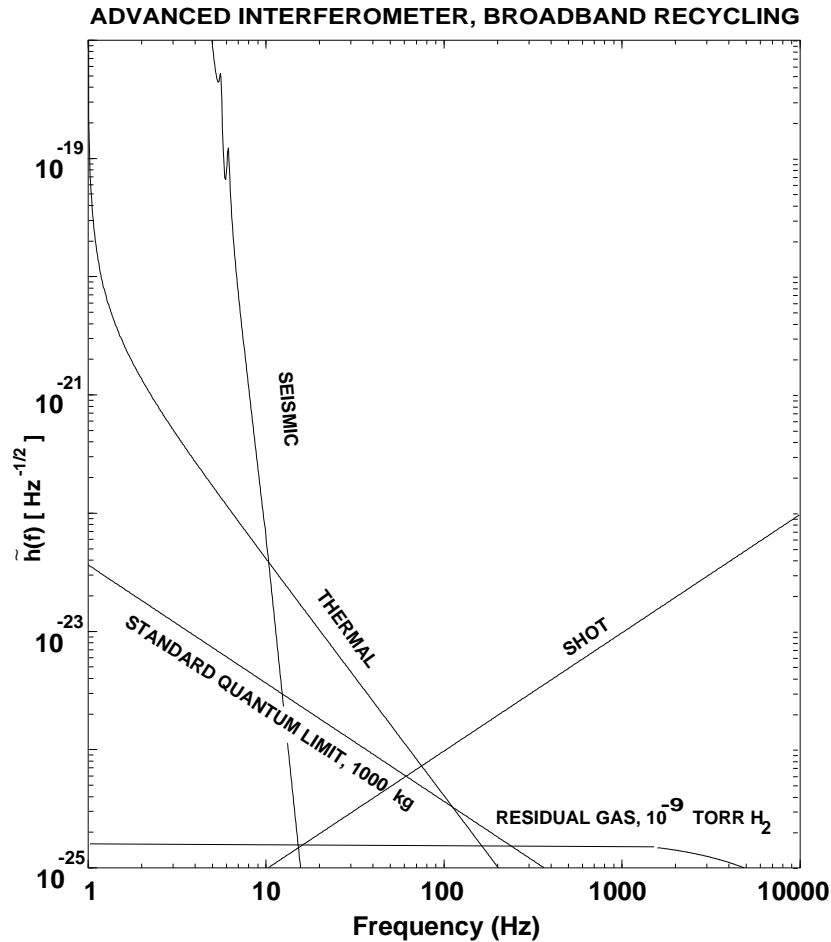


Figure 8: Advanced Interferometer Sensitivity

ferometers, $h_{sn}(f \ll f_o) \approx 10^{-24} (1/\sqrt{Hz})$.

An optical power of 6 W @ $\lambda = 1064$ nm for the initial interferometer will result in a shot noise equivalent strain of $h \approx 10^{-22} (1/\sqrt{Hz})$.

The frequency dependence of the shot noise due to the cavity pole, can be obtained by using the (optical phase)/(GW strain) transfer function above. For the case with no recycling ($G_R=1$):

$$h_{sn}(f) = f_o \left(\frac{h\lambda}{\eta \epsilon P (1 - L_{opt}) c} \right)^{1/2} [1 + (f/f_o)^2]^{1/2}$$

where a factor of 2 has been incorporated to account for recovery of phase information from the RF modulation techniques used in a practical interferometer. When power recycling is included, assuming the optimum condition wherein all of the optical loss in the system is due to loss in the cavity mirrors, then $G_R = 1/L_{opt} = L/(4Ac\tau_s)$ where A = average loss per mirror, and

$$h_{sn}(f) = \left(\frac{f_o c A}{\pi L} \right)^{1/2} \left(\frac{h\lambda}{\eta \epsilon P (1 - L_{opt}) c} \right)^{1/2} [1 + (f/f_o)^2]^{1/2}$$

Shot noise is mitigated through the use of resonant cavities and power recycling. Further reduction in the shot noise component requires increased laser input power (technology driven) and/or utilization of squeezed-state light [21].

Thermal Noise

According to the fluctuation-dissipation theorem of statistical mechanics [22], any damping mechanism in a physical system is accompanied with thermally-driven random fluctuations in the system's modes of motion. The damping mechanism for the LIGO suspension

system is structural (material) damping associated with the flexure of the suspension wires (principally at the attachment restraints) and the internal "drum head" modes of the mirrors [23]. The brownian motion produced by the thermal noise has $kT/2$ kinetic energy per degree of freedom with a resulting rms motion:

$$x_{rms} = \left(\frac{kT}{M\omega_o^2} \right)^{1/2}$$

where ω_o = natural frequency, k = Boltzmann constant, T = temperature and M = effective mass in the degree of freedom (mode) with frequency ω_o .

The suspension wire resonances ("violin modes") are excited by the thermal noise [24]. While it is desirable to place these resonances outside of the LIGO observation band, other considerations constrain the design. The need to maximize the modal quality factors, Q_s , so that the thermal noise floor away from resonance is below the LIGO detection goals, suggests minimizing the diameter of the suspension wires. However, strength considerations provide a lower limit on the smallest practical diameter (and correspondingly the lowest frequency to ~ 500 Hz). The structural damping associated with the wire resonances results in $Q_s > 10^4$. In addition, the recoil term, $M_{wire}/M_{mirror} = 10^{-4}$ attenuates the effective strain amplitude of wire resonance noise.

Since the suspension wire modes are within the measurement band for LIGO, these modes have to have very high Q (low damping) so that their effect is limited to narrow regions in frequency and can be filtered out of the measurements in post-processing. Thermal noise in the suspension wires is mitigated through proper design of the attachment points of the wires (where bending stresses and damping is highest), minimizing the diameter of the wire (subject to stress limitations and the effect of "excess noise" discussed below).

Thermal noise also induces brownian motion in the last stage of the seismic isolation stack. The seismic isolation system has a low Q (~ 1 - 3 by viscous damping) and a low first resonance (~ 1 Hz) by design (for seismic isolation reasons discussed below). This results in a residual strain of

$$h_{st}(f) \sim 10^{-25} \left(\frac{2000}{f} \right)^2 (1/\sqrt{Hz})$$

above the resonance. The $1/f^2$ dependence of the suspension thermal noise is a result of the pendulum resonance.

The mirror (test mass) with the dimensions given in Table 3 has a first internal resonance of about 10 kHz. For a monolithic fused silica mirror the Q has been measured as $> 10^6$ and the damping mechanism has been shown to be structural damping (i.e. frequency independent). The resulting equivalent strain is

$$h_{imt}(f) \sim 10^{-24} \left(\frac{10000}{f} \right)^{1/2} (1/\sqrt{Hz})$$

below the resonance. The $1/\sqrt{f}$ dependence of the test mass thermal noise is due to the nature of structural damping (whereas viscous damping has no frequency dependence below the resonance, as indicated in Figure 9).

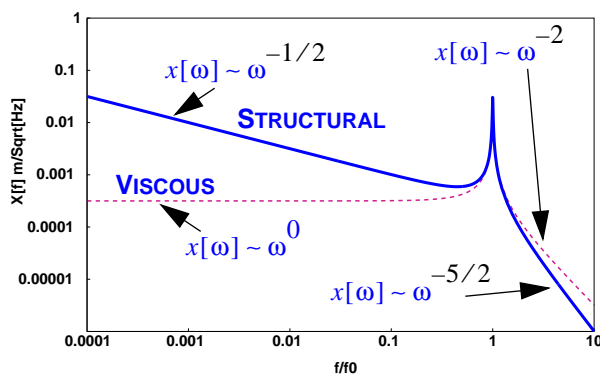


Figure 9: A comparison of viscous and structural damping

“Excess” Noise

All materials under load will creep or flow.

Glass for example is essentially a very viscous fluid at room temperature and flows under stress; this is why old glass windows are thicker on the bottom than the top. Static loads on metals, especially near the yield stress, will cause diffusion of dislocation boundaries. This process is not constant in time, but rather manifests itself as discrete (non-Gaussian), statistical events. These strain relief jumps in the suspension system can cause sudden mechanical shocks. Experience in the 40 m prototype system suggests that if the stress in the suspension wires is less than 1/2 of the ultimate stress, this phenomenon is not observable. Concern about this effect in the wires for advanced interferometers and in bolted assemblies, where the bolts may undergo strain relief, has prompted further on-going experimental study [25].

Seismic Noise

The design for seismic isolation in the initial interferometer systems is a passive stack of four mechanical low pass, critically damped filters topped by a single pendulum. Each stack acts as a second order system giving a $1/f^2$ roll-off above the resonance:

$$h_s(f) = \frac{\delta x_{ambient}(f)}{L} \left(\frac{f_s}{f} \right)^{2n} \left(\frac{f_p}{f} \right)^2 (1/\sqrt{Hz})$$

where f_s is the stack resonance frequency, f_p is the pendulum frequency and n is the number of layers in the seismic isolation stack and $\delta x_{ambient}(f)$ is the ambient base motion disturbance spectrum. For the parameters of the initial interferometer,

$$h_s(f) = 10^{-25} \left(\frac{90}{f} \right)^{12} (1/\sqrt{Hz})$$

based upon a conservative estimate of seismic disturbances at the selected sites.

Gravity Gradients

Atmospheric motion, ocean tides and earth micro-seismic motion (earth “tides”) represent

low frequency sources of noise which are not attenuated by the seismic isolation system. As the isolation systems improve beyond the initial passive design, these noise sources will represent a practical (though not fundamental) low frequency limitation to gravitational wave measurement. Based upon measurements, the following is the expected frequency variation in this noise term:

$$h_{gg}(f) \sim 10^{-25} \left(\frac{12}{f}\right)^4 (1/\sqrt{Hz})$$

Although the initial interferometer is not sensitive to the gravity gradient due to the motion of a person walking in proximity of a test mass, advanced interferometers are projected to be sensitive to this noise source to a distance of 10 m [26].

Residual Gas

The mechanical effects of an intervening gas, such as acoustic coupling to the environment and damping of the suspensions, are mitigated to a negligible level in LIGO by operating at a pressure of 10^{-6} torr. However, fluctuations in the forward scattering of laser light by residual gas particles is a potentially more serious noise source. The scattered field of individual gas molecules causes pulses in the photodetector as the molecules pass through the interferometer beam. The equivalent gravitational strain noise derived from the average power spectrum of the pulses produced by the molecules residing in the beam is [27]:

$$h_{rg}(f) = \frac{4\pi\alpha}{L} \sqrt{\frac{2\rho_n}{v_o}} \left[\int_0^L e^{\frac{-2\pi f w(z)}{v_o}} \frac{1}{w(z)} dz \right]^{\frac{1}{2}}$$

where L is the arm length (beam path length), α is the polarizability of the residual gas molecule at the optical frequency ν , ρ_n is the average number density of the molecules, v_o is the average thermal velocity of the molecule and $w(z)$ is the beam's Gaussian radius as a function of the coordinate along the beam axis, z .

The noise due to residual gas is nearly independent of frequency within the LIGO measurement band and hydrogen is the dominant contributing gas species. This gas scattering model has been confirmed by experiment [28] for dependencies with respect to pressure (number density), molecular polarizability and molecular mass (i.e. the thermal velocity of the molecule at a given temperature).

Standard Quantum Limit

Light reflecting from the test masses imparts forces due to its momentum. Fluctuations in the amplitude of the laser thus cause random forces on the optics. The forces due to intensity fluctuations are symmetric between the two arms so that the effect cancels except for unintentional mechanical and optical asymmetries.

In addition to these symmetric radiation pressure fluctuations, there are uncorrelated pressure fluctuations between the arms [29]. Quantum electrodynamic vacuum fluctuations that enter the interferometer through the dark side of the beam splitter, superimposed with the main beam's electromagnetic field, are one source of the "standard quantum limit" for the gravitational-wave detector and are a macroscopic example of the "Heisenberg microscope". Since the fluctuating radiation pressure is proportional to the correlated product of the vacuum field and the laser field, it varies as the square root of the laser power and fluctuates on time scales of the cavity storage time, a characteristic time for the vacuum electric-field fluctuations to change phase by π relative to the laser field. There is an optimum laser power since the radiation pressure noise varies directly as the laser power and the sensing noise varies inversely with the laser power. The net pressure and sensing noise at the optimized laser power can be shown to be [29]:

$$h(f)_{QL} = \sqrt{4/\pi} \left(\frac{h}{m}\right)^{1/2} \left(\frac{1}{2\pi f L}\right) (1/\sqrt{Hz})$$

The quantum noise is not a factor in the initial interferometer designs but does set a fundamental limit to the technique and is one of the sources of noise that argues for a long arm length.

6. IMPLEMENTATION/DESIGN

In the following subsections, the facilities, vacuum system, and detector system design and status as well as supporting research and development activities are discussed.

Facilities

Each site will consist of a large corner station building complex, which includes a building to house the lasers and vertex interferometer optics and vacuum equipment (the Laser and Vacuum Equipment Area or LVEA) and an Operations and Support Building (OSB) to house the control rooms, supporting labs and offices (Figure 10). Each site will also have

two end station buildings which house a Vacuum Equipment Area (VEA) for the optics and vacuum equipment associated with the end masses of the two arms, as well as supporting labs and preparation areas. At the Hanford site, there will also be mid-station buildings on each arm to house the VEAs for the 2 km long interferometer; At the Livingston site the mid-stations will be small and simple shelters to house some vacuum valves and pumps. The LVEA and VEAs are large and clean laboratory spaces (clean room construction practices, high bay with 15m hook height) with material handling systems.

The vacuum enclosure between the corner, mid- and end-stations is accomplished with a welded stainless steel beam tube. Since the steel tube is thin walled and vulnerable, it is housed in an enclosure which permits manned access. The Beam Tube Enclosure (Figure 11) is built up from 3.0 m long cast concrete sec-

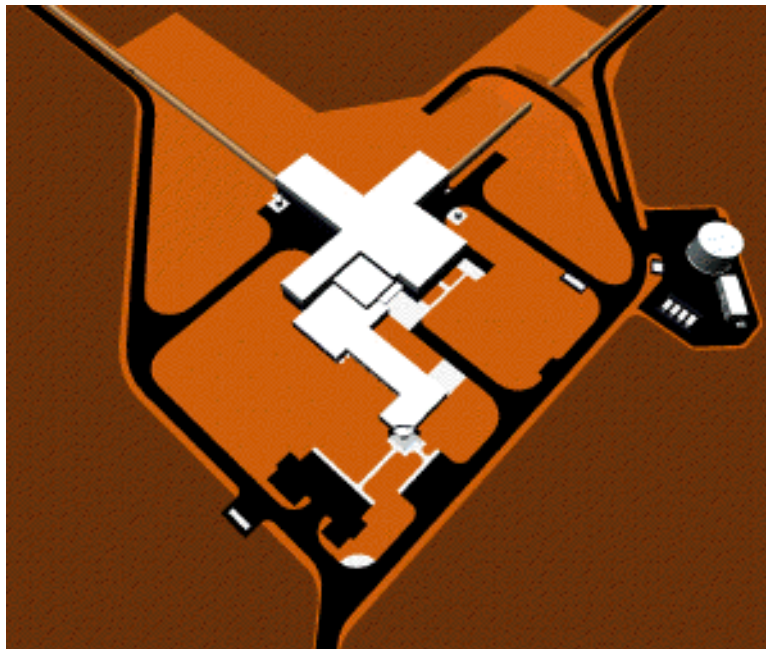


Figure 10: Corner Station Site Layout

The beam tube enclosure arms extend beyond the drawing in the upper left and right corners to the mid-station at 2 km distance and the end-station at 4 km. The X-shaped building at the vertex of the two beam tube arms is the Laser and Vacuum Equipment Area (LVEA) (~ 90 m long). The lower building in front of the LVEA is the Operations Support Building where the control room, data storage and support laboratories are housed.

tions with an semi-elliptical cross-section having a height of 2.7 m and a width of 4.0 m. In addition to providing the beam tube protection from the elements and stray bullets from hunters, it affords some degree of passive temperature control by blocking direct view of the sun and providing a significant thermal mass to mitigate temperature excursions.

Key design implementation considerations for the facilities are:

- selection of a seismically quiet site
- design of the building infrastructure to minimize vibration and acoustic noise through careful design of the foundation slab and the design and location of heating, ventilation and air-conditioning equipment
- proper grounding and shielding and isolation of EM noise sources

Both sites have been cleared and the Hanford site has been graded along the extent of the 4 km arms and is awaiting settlement before construction activities commence. Final grading of the Livingston site is currently underway. The final design of the BTE has been accomplished and the process for selecting a construction contractor is underway. The building design has just passed the preliminary design review milestone, with an April 1996 completion of the final design expected. Ground breaking for the construction activities is planned for July 1996.

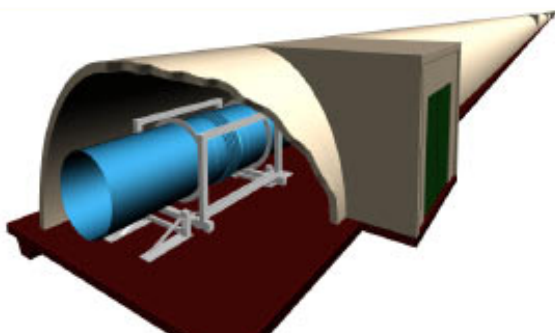


Figure 11: Cut-away view of the Beam Tube in the Beam Tube Enclosure

Beam Tubes

The LIGO beam tubes are fabricated by the same method used to make oil pipelines. The tube is fabricated from rolled sheet stock by helically winding and welding it with a machine designed expressly for this operation. The characteristics of the beam tubes are:

- module lengths of 2 km
- tube diameter of 1.22m (1 m clear aperture after baffling)
- internally baffled to reduce scattered light phase noise
- very low allowable air leakage rate ($< 10^{-9}$ atm cc/s, He)
- very low outgassing rates:
 - the pressure for advanced interferometer applications $< 10^{-9}$ torr (All residual species)
 - the outgassing rate for H_2 must be $< 10^{-13}$ torr-liters/cm²/s
 - the outgassing rate for H_2O must be $< 10^{-15}$ torr-liters/cm²/s
 - partial pressures for $CO + CO_2 + H_{2N}C_N +$ higher order hydrocarbons, must be even lower

Since there will be approximately 100 km of welds (depending upon beam tube skelp width), quality control and cleanliness must be pursued diligently throughout the fabrication and integration process in order to insure low leak rates, long lifetime and no virtual leaks.

A prototype fabrication effort has been successfully concluded with a qualification test which demonstrated successful cleaning procedures, leak testing procedure ($< 10^{-11}$ atm cc/s), and bakeout procedures. The production effort for 16 km of beam tube is about to commence.

Concurrently, research into baffling material optical properties and mechanical design is continuing. The baffles are expandable, truncated conical fustrums which are friction fitted

into the inner diameter of the beam tube at approximately 300 locations per beam tube arm. The interior edge of the baffle is serrated in a random sawtooth profile in order to minimize diffraction effects. The surface which faces the test masses is coated with a material which is absorptive at the laser wavelength; The most promising candidate to date is a “black glass” coating which is fired onto the stainless steel substrate. This material is used in the household oven market and provides an affordable, durable and highly absorptive and specular surface. Tests to confirm its vacuum compatibility are underway.

Vacuum System

The LIGO Vacuum System (Vacuum Equipment + Beam Tubes) provides:

- A clear aperture for the interferometers
- Very large aperture gate valves to isolate 1.22 m beam tubes
- A clean environment for the precision optics
- Chambers with easy access for installation and maintenance, repair and upgrades to the optics
- A low pressure in order to minimize dif-

fraction and acoustic coupling

- Extensive controls and monitoring equipment to ensure safe and efficient operation
- High pumping speeds and large volumes — beam tube pumping is accomplished from the 4 km ends

The LIGO Vacuum System will be the world’s largest ultra-high ($< 10^{-9}$ torr) vacuum system with a pumped volume of roughly 20,000 m³. The large chambers which house the optics (depicted in Figure 12) are unique to LIGO and have been designed with maximum port access for external viewing and alignment systems as well as large ports for easy installation. A preliminary design review of the vacuum equipment was successfully concluded recently and final design efforts are well underway

Detector

The baseline detector systems employs techniques proven on the 40m and 5m prototype systems at Caltech and MIT respectively. R&D experiments on optical recombination and power recycling are being performed to gain insight and confidence in the technical approaches to be used on the LIGO system.

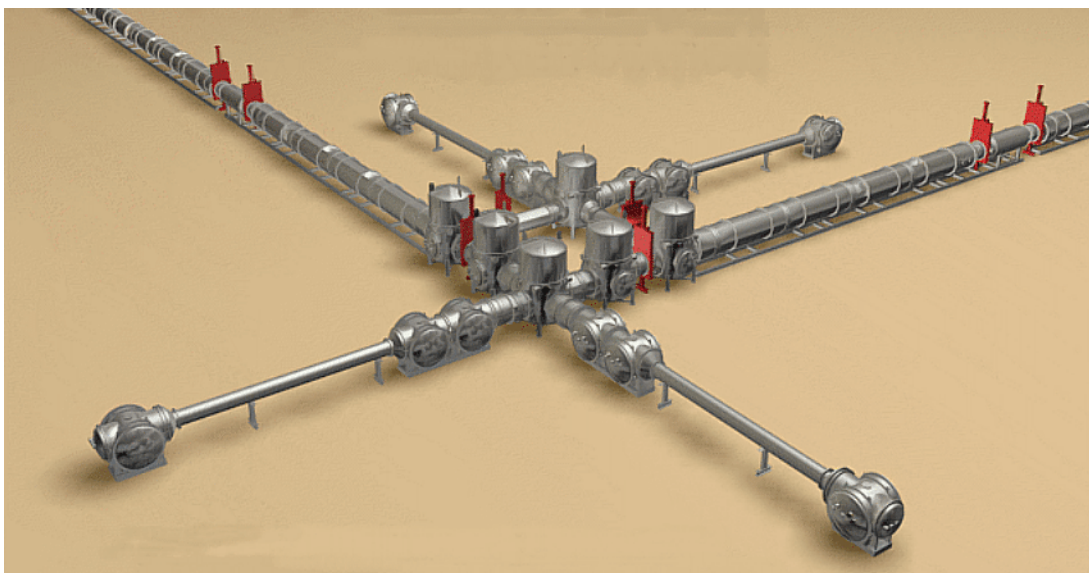


Figure 12: Vacuum equipment layout in the Hanford corner station

The long history of prototype development and incremental reduction in, and improved understanding of, the noise floor and the required precision engineering enables the team to implement the LIGO system with low risk and transition from an R&D system to a “turnkey operation” required of an observatory.

Core Optics — Collaborative studies with industry and on mirror polishing, coating and metrology have been initiated. LIGO requirements are for high reflectivity (1 ppm loss) and optically flat ($\lambda/600$ rms) surfaces over the central 15 cm diameter of optics as large as 25 to 30 cm in diameter and up to 10 cm thick (~ 25 kg). The required reflectivity has been achieved in preliminary tests with a 34 layer dielectric coating.

Polishing manufacturers report the capability to polish to $\lambda/800$ rms (@ $\lambda=633$ nm) using conventional pitch polishing as well as teflon lap polishing. Since these levels are pushing the limits of metrology, an independent effort in establishing the performance of as-built optics has been initiated with the National Institute of Standards and Technology (NIST).

Seismic Isolation System — The baseline approach for seismic isolation [30] is a four stage, passive, cascaded mechanical filter (Figure 13). In the prototype systems built and tested at MIT and employed in the 40 m prototype at Caltech, each stage is comprised of a monolithic stainless steel block (with a high first vibration frequency). Between each layer are an array of elastomeric spring dampers (Figures 13 and 14). The springs have been fabricated from a fluoro-carbon elastomer (Viton). The visco-elastic behavior of the spring elements are exploited to provide high damping of the stack normal modes ($Q \sim 3$)

while also yielding a rapid rolloff of the stack transmission above the stack modes. Comparisons between experiment and 3D finite element models are used to gain an understanding and modeling capability to enable scaling the concept for the full scale LIGO system.

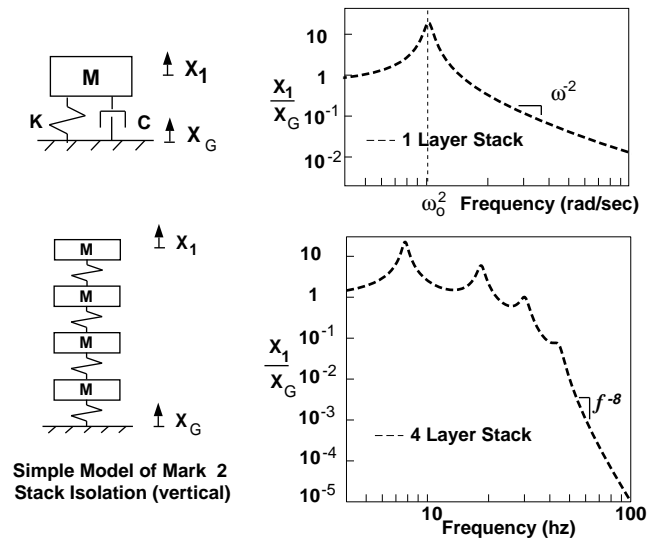


Figure 13: Passive Isolation Concept.

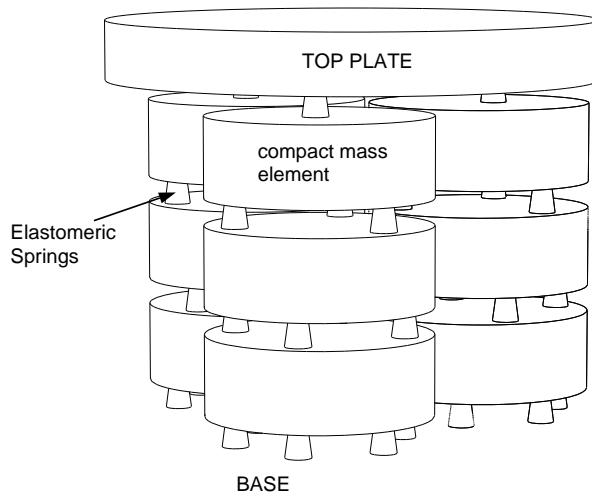


Figure 14: Prototype isolation stack
A single circular tale is supported through springs by three isolating legs of three mass-spring layers each. Overall height of 68 cm and the width of 78 cm for the prototype system.

Tests of the degradation of the reflectivity of mirrors exposed to the elastomer indicate < 0.3 ppm/week (at the 95% confidence level) [31]. While this result is close to LIGO anticipated requirements, improvements in the design which would eliminate exposure of the optics from outgassing of the elastomer are being sought. One approach under investigation is to use a metallic spring with constrained-layer damping, such that the elastomer is sealed from exposure to the vacuum. Active vibration isolation techniques have also been explored [32] and are likely candidates for advanced interferometers.

Suspension System — Further attenuation of the base motion vibration is afforded by the pendulum suspension of the test mass (Figure 15). The test mass is suspended from a control block by a loop of wire sized so that it is

loaded to $\sim 1/2$ its breaking strength (75 micron-diameter steel music wire is used in the 40 m prototype). The magnetic/coil actuators on the control block are used to damp angular motion of the suspended test mass, on the basis of optical lever system measurements. Longitudinal motion, sensed by an edge detector, is damped by a piezoelectric actuator. The large forces required for lock acquisition (and interferometer response calibration) are achieved with magnets attached directly to the test masses and nearby coils. A photograph of the test mass suspension used in the 40 m prototype interferometer, mounted on a seismic isolation stack in a vacuum chamber, is shown in Figure 16.

The suspension system for LIGO is designed to handle a variety of optics including the test masses, beamsplitters and mode cleaner mir-

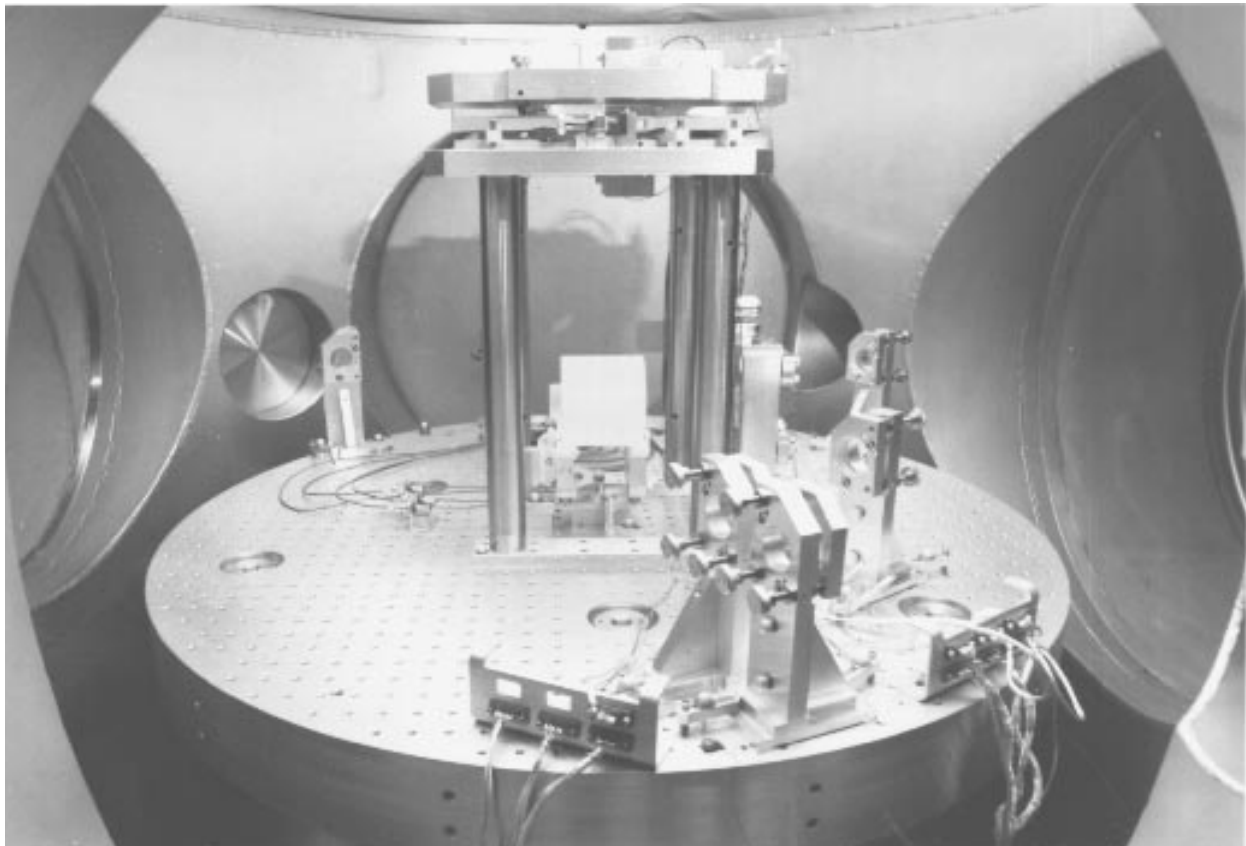


Figure 16: Photograph of a test mass suspension, mounted on a vibration isolation stack, inside the 40 m prototype interferometer vacuum system

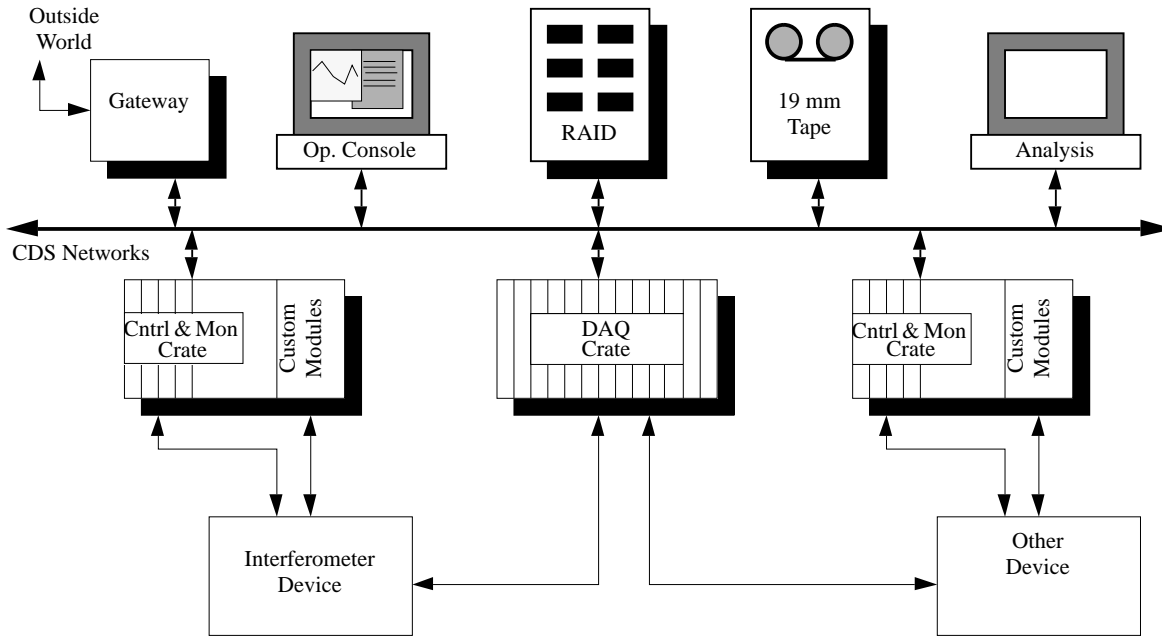


Figure 17: Control and Data System Block Diagram

rors, ranging in size from 7.5 cm diameter to ~25 cm diameter and 0.2 kg to ~ 25 kg. The longitudinal motion dynamic range requirements vary from $\sim 10^{-5}$ m peak-to-peak (pp) at

0.1 Hz to $\sim 10^{-16}$ m pp at 1 kHz in operation (and to $\sim 10^{-11}$ m pp at 1 kHz during lock acquisition). The experience gained with the 40 m interferometer is essential to achieving the design requirements of the suspension system. A number of improvements have been incorporated into the design for the full scale system, such as a single wire-loop suspension, angular and length control through a common set of magnet/coil actuators resulting in a less complicated transfer function.

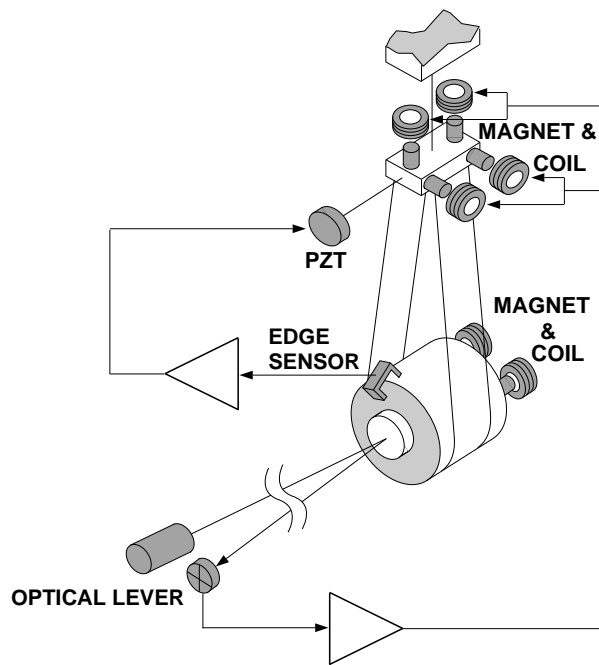


Figure 15: Schematic of a suspended test mass and its control hardware (40m interferometer design)

Control and Data System (CDS) — The LIGO CDS system is an advanced control and data system using state-of-the-art network architecture and hardware components. The CDS provides (Figure 17):

- Operator consoles in the control room of the Operations Support Building designed to have multiple heads and to be interchangeable,
- Local/portable consoles for use in each building
- a Rapid Array of Inexpensive Disks (RAID) used for storage of system parameters and data

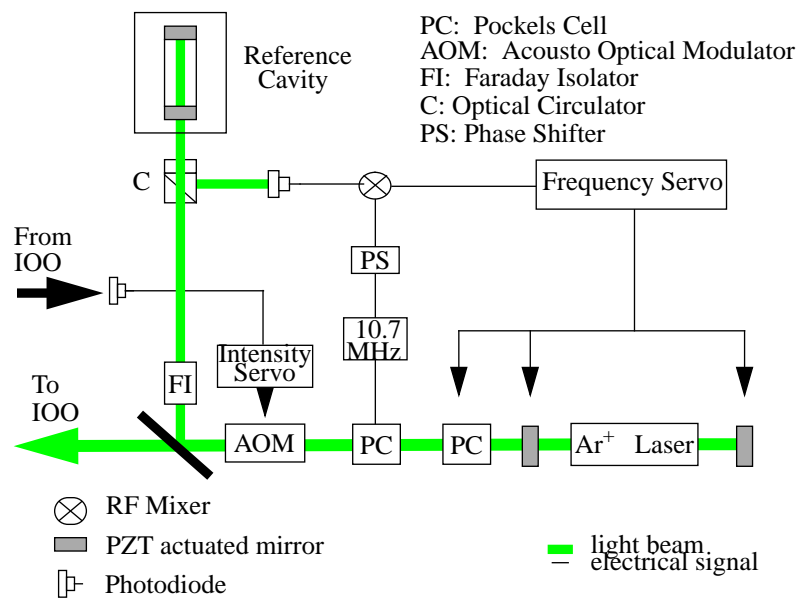


Figure 18: Prestabilized Laser System

- tape units for storage of archived data from the data acquisition system
- analysis stations to be used for preliminary on-site data-analysis and possibly filtering and generation of triggers
- high speed, fiber-based networks for data acquisition and lower speed for executive control and monitoring
- Control and Monitoring standard VME crates with custom analog modules for local servo-control
- Data Acquisition (DAQ) Crates: standard VME crates with processors, waveform digitizers, timing generation and communications modules

Sample rates for the DAQ system range from < 1 sample/sec to ~ 20 K samples/sec (the GW signal rate). The current data rate estimate is 6 Mbytes/sec per interferometer.

In addition to control and monitoring of the basic interferometer detector, the CDS handles control and monitoring of the vacuum equipment, remote diagnostics and physics/environmental monitoring (PEM). The PEM data is used for veto of erroneous GW events.

Prestabilized Laser System (PSL) — The PSL provides a single-mode, single-frequency beam > 4 W to the input optics subsystem. The prototype PSL servo-control system has achieved the following stability parameters for an argon-ion laser ($\lambda=514$ nm):

- frequency stabilization $\Delta f/f \sim 10^{-15}/\sqrt{Hz}$
or $< 1 \text{ Hz}/\sqrt{Hz} @ 100 \text{ Hz}$ (achieved with a gain of 10^5)
- intensity (amplitude) fluctuations $\Delta P/P \sim 10^{-7} 1/\sqrt{Hz}$ (achieved with a gain of 10^3)
- beam angular jitter to $< 200 \mu\text{rad}/\sqrt{Hz} @ 100 \text{ Hz}$
- polarization fluctuations in the beam to $< 10^{-6} 1/\sqrt{Hz} @ 100 \text{ Hz}$

The PSL is built around a commercially available Ar^+ plasma tube laser which has been extensively modified for stability control. (The PSL is in the process of being redesigned for use with a Nd:YAG laser ($\lambda=1064$ nm) as a consequence of a recent decision to switch to a solid state laser.)

A block diagram of the PSL system is given in

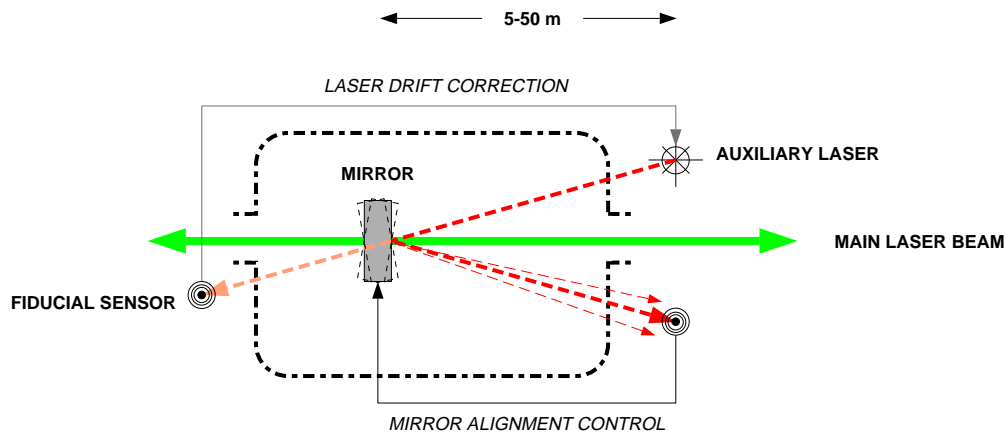


Figure 19: Three-point optical lever

Figure 18. Amplitude (intensity) control is accomplished with an acousto-optic modulator based on feedback from sensing of the light transmitted through the mode cleaner. Phase noise is controlled by phase shift control of a Pockel cell modulator, where the servo-control signal is derived from demodulation of the output of a photodetector positioned to look at the reflected light from the reference cavity (i.e. a “reflection locking” technique). This reflection locking signal is also used to slave the laser cavity to the reference cavity by PZT actuation of the cavity mirrors.

The PSL frequency and intensity servo-controls are operational under computer control in a manner identical to what is intended for LIGO. The PSL control interface has been developed with a software system, called EPICS, developed by Los Alamos National Labs explicitly for control of large, complex instrumentation. The system performs control of the laser, the servo-controls, data monitoring and archival and alarm handling. Testing of the PSL prototype for noise performance, availability and environmental sensitivity (seismic noise, acoustic noise and temperature variations) is underway.

Alignment Sensing and Control (ASC) — The ASC subsystem provides both initial align-

ment and operational alignment of the LIGO interferometer optical elements. The initial alignment is required to take the interferometer from an arbitrary misaligned state to a condition where the operational length and alignment systems are functional. The initial alignment will utilize optical referencing from GPS-located monuments.

Automatic maintenance of alignment during operation as currently conceived involves three principal subsystems:

- An optical level system (Figure 19) will be used to maintain angular alignment over short time periods (10-100 sec) through closed loop servo-control. (The time limitation reflects the time scale for dimensional stability of the common isolated foundation.) The optical lever has successfully employed in the 40 m prototype system.
- A centering system to minimize cross-coupling of angular noise to length noise.
- A wavefront sensor for use in determining the optimal alignment with an update rate of about 10 sec. The phase front sensors are quadrant photodiode detectors with holes in the center. The alignment signals (proportional to the amplitude of the light not in the TEM_{00} mode) are derived from

the differences between opposite quadrants of the photodiodes [18].

Length Sensing and Control (LSC) — The LSC system performs the measurement and control of the arm cavity lengths and the recycling cavity lengths (i.e., the 4 key lengths of the interferometer). The LSC must first acquire lock (resonance) of the cavities before transitioning to an operational mode. The control for lock acquisition is highly nonlinear [33] whereas the operations mode is in a small signal, linear control regime.

Research & Development

Current LIGO R&D effort is dominated by support to the design and development of the initial detector system. Future efforts will be aimed at enhancements to the initial detectors. The R&D efforts are predominantly

related to three interferometer systems:

- the 40 m interferometer: presently being used for length control in operation and during acquisition (nonlinear regime)
- the Phase Noise Interferometer (PNI): a 5 m long interferometer used for phase noise studies and development of photodetector/demodulation systems, and
- the Fixed Mass Interferometer (FMI), a testbed for length control configuration tests and alignment control studies based on wavefront sensing

40 m Prototype — The 40m Interferometer (Figure 20) was recently reconfigured to include optical recombination (previously the signals from the two arms were combined electronically) and a revised modulation and control system in order to be more representative of the full scale system and to test models for the dynamics of length control. In the near

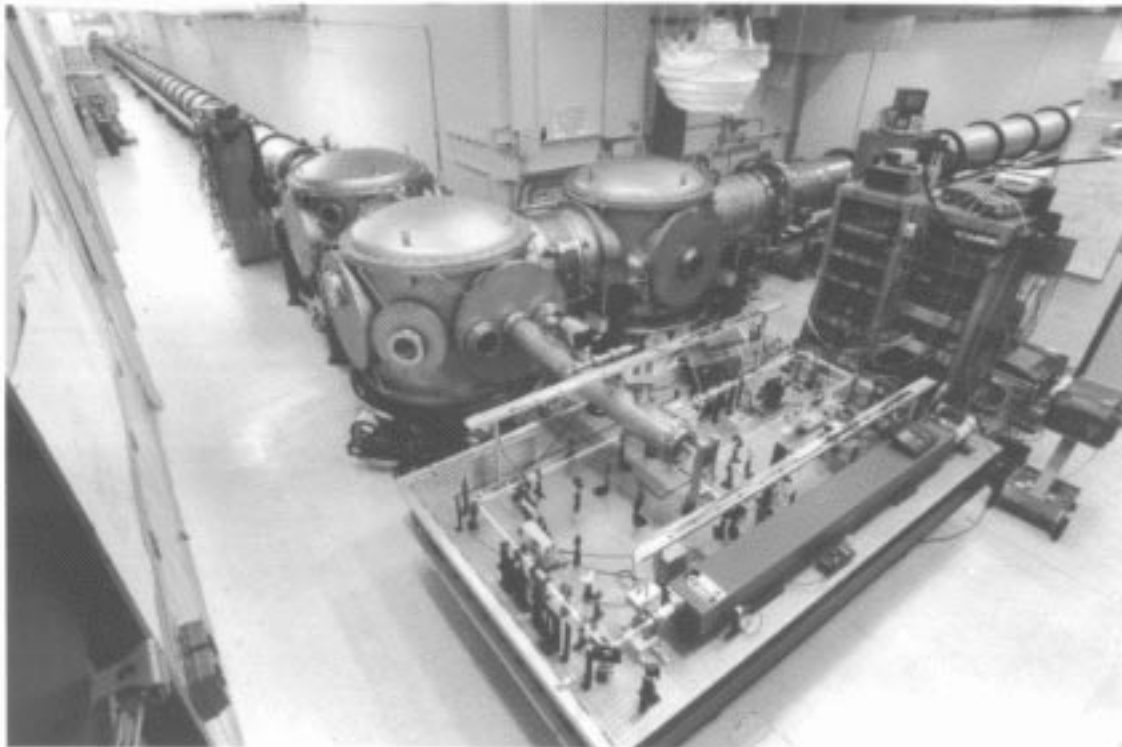


Figure 20: 40-m Interferometer

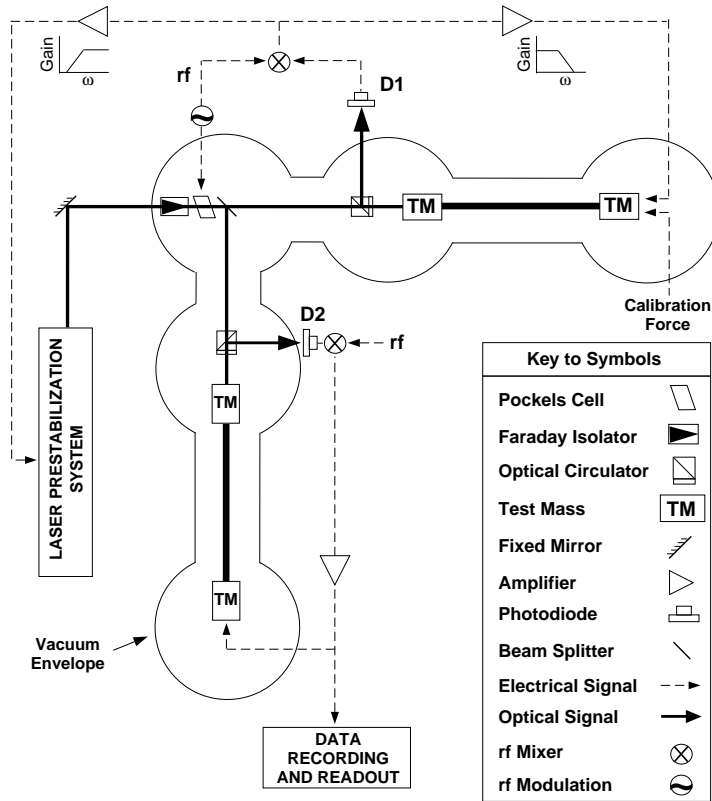


Figure 21: 40 Meter Prototype Configuration

future a recycling mirror will be added to complete the reconfiguration. The present 40 m configuration is shown schematically in Figure 21. The two arms are 40 meter long Fabry-Perot cavities formed by mirrors suspended with a 1 Hz pendulum frequency from vibration isolated platforms. Light from an Argon ion laser operating at 514.5 nm, capable of producing a single mode output power up to 5 W, strikes a beamsplitter illuminating both cavities. The laser is locked in frequency to an optical resonance of the first arm using a reflection-locking technique [19]. The second arm is held in resonance with the laser light by a servo-system which exerts forces on the end test mass using a magnetic drive. Differential forces on the test masses, such as those produced by a gravitational wave, are sensed by recording the feedback force needed to keep the second arm on resonance.

The 40 m interferometer has been under devel-

opment since 1982 [34], [35]. The recent evolution of its noise spectrum as the interferometer has been improved is shown in Figure 22. The improved performance of the system over time is the result of controlling measurement and control noise and increasing the optical power delivered to the cavities. The largest improvement in the displacement sensitivity achieved to date was the result of redesigning the seismic isolation stacks to give ~ 2 orders of magnitude lower transmission at 100 Hz. At frequencies between 500 Hz and 1000 Hz, the initial (Mark I) interferometer was limited by mirror surface fluctuations due to thermal noise in the test masses. The Q s of these mirrors (800 to 54,000) were much lower than expected, probably as a consequence of bonding mirrors to the fused silica substrate; the new

test mass mirrors are a monolithic construction, with the coating applied directly to the substrate. The measured Q s of the new test masses range from 4.0×10^4 to 8.1×10^6 , giving a predicted improvement of nearly an order of magnitude in the thermal noise contribution to the spectrum.

The new test masses also have reduced optical losses compared with the older mirrors, resulting in higher stored power and a reduced shot noise component to the spectrum. The interferometer is shot noise limited at frequencies above 1 kHz.

A comparison of the measured sensitivity of the 40 m interferometer with predicted performance is shown in Figure 23. The seismic noise prediction is an empirically based prediction using measured base motion spectrum and the transfer function from floor motion to interferometer output. The thermal noise pre-

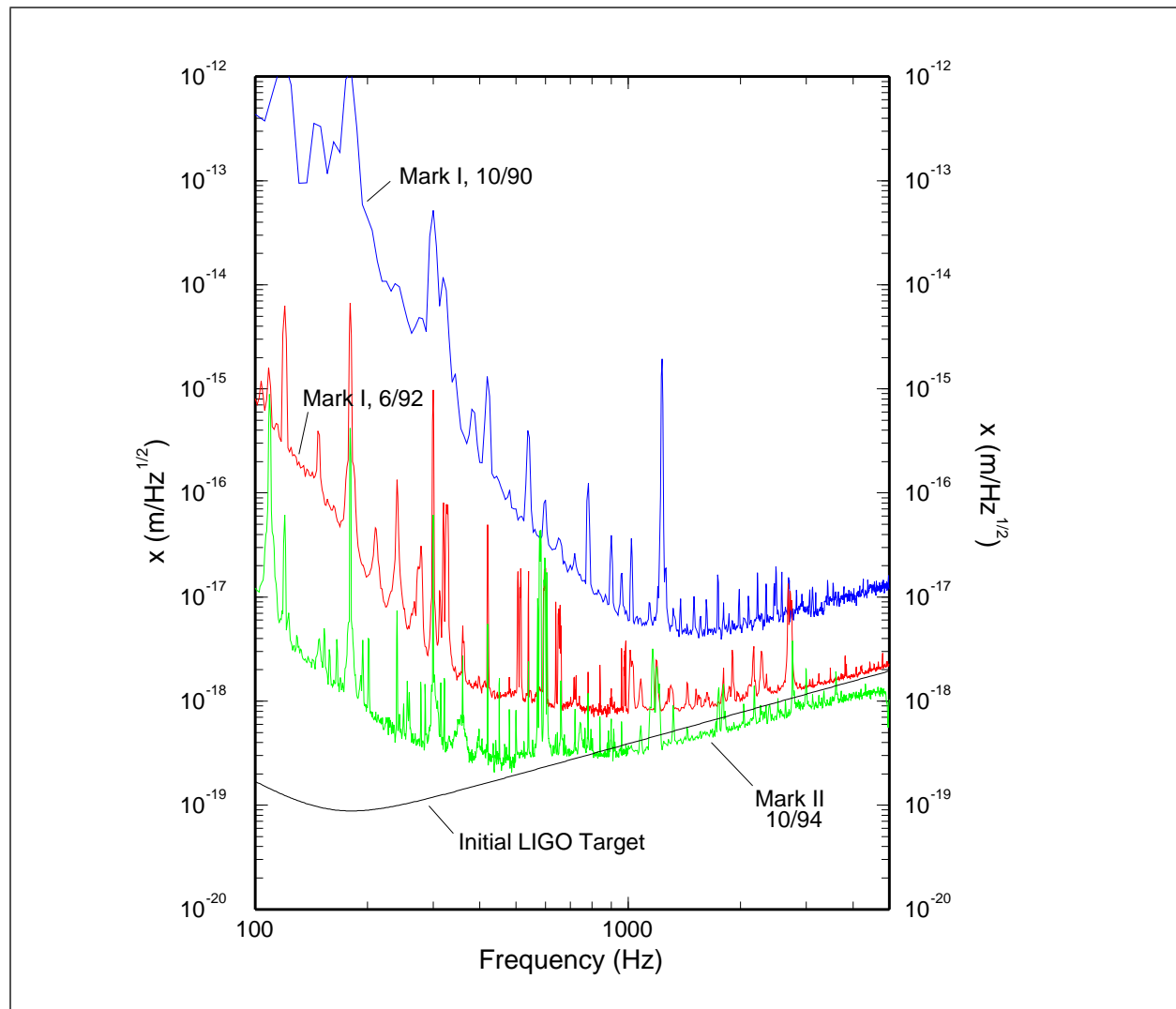


Figure 22: Progressive improvement in the displacement sensitivity of the 40-m interferometer

diction is theoretical, based upon measured frequencies and Q s for various modes. The theoretical shot noise curve has been confirmed experimentally to within $\sim 20\%$. The “line” features, or spikes, in the spectrum are either due to wire resonances (marked “W” in Figure 23), suspension mechanical resonances (marked “S”) which will be eliminated in a planned upgrade of the suspension system, and powerline frequency harmonics. The disagreement between theory and experiment between 100 Hz and 500 Hz is of unknown origin and is currently under investigation. The noise spectrum of Figures 22 and 23 is the best achieved to date with the 40-m interferometer and corresponds to a best displacement sensitivity of 2.5

$\times 10^{-19} \text{ m}/\sqrt{\text{Hz}}$ near 450 Hz.

Phase Noise Interferometer — The intent of the PNI program is to demonstrate LIGO’s required a phase sensitivity $< 10^{-10} \text{ rad}/\sqrt{\text{Hz}}$, by achieving a circulating power level of 70W, approximately the same level as required in the initial LIGO interferometer. The system will initially be in a non-recycled Michelson configuration (Figure 24) with 1 W of optical power, then recycling will be added to increase the power to 15 W, and finally a mode cleaner will boost power to 70 W. The PNI will also be used to investigate scattered light control. The PNI system (including an active vibration

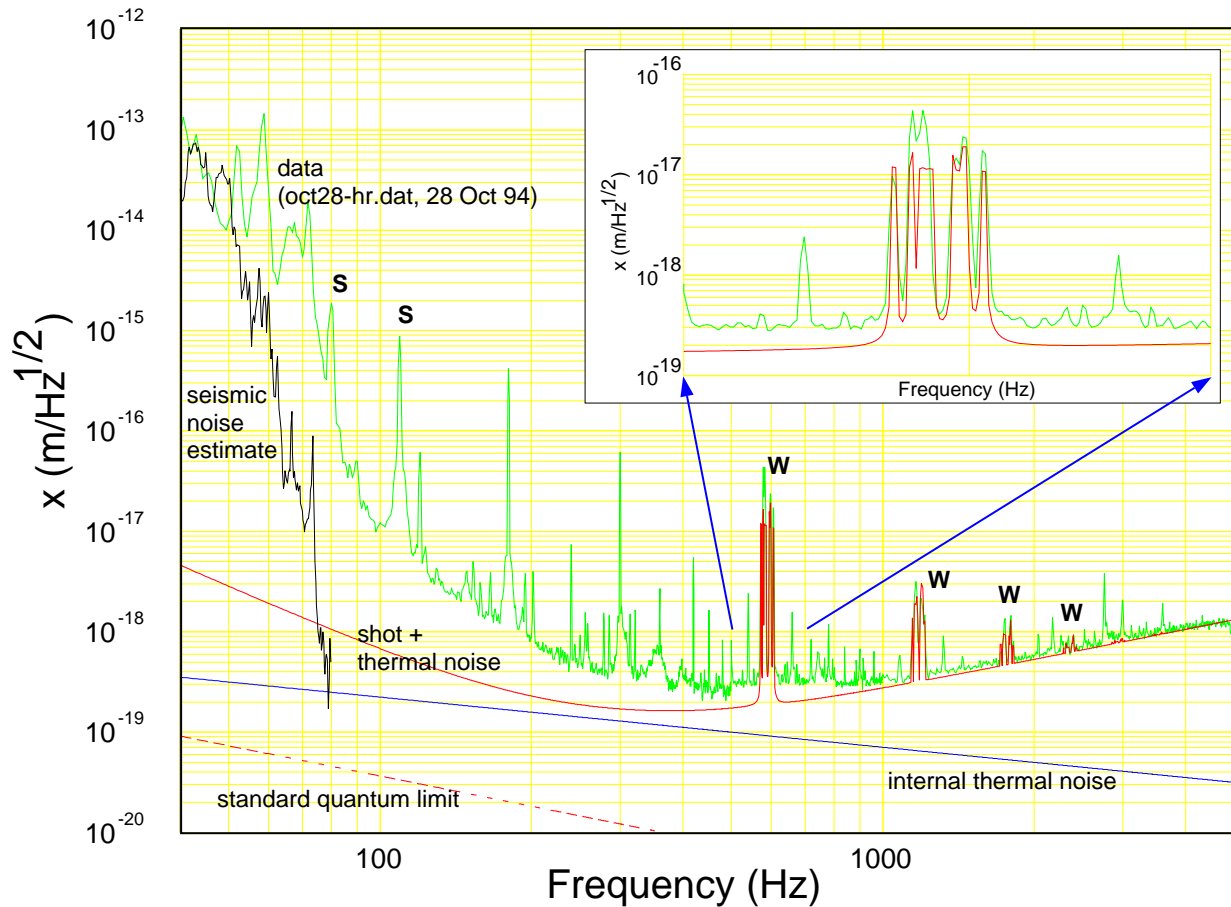


Figure 23: Displacement Sensitivity of the 40 Meter Prototype Interferometer

isolation system) has been integrated at MIT and has achieved $8 \times 10^{-9} \text{ rad}/\sqrt{\text{Hz}}$ to date in the Michelson configuration. A recycling mirror will be added to the system soon.

Fixed Mass Interferometer — The FMI is being set up to perform initial tests of the frequency-shifted, subcarrier length sensing configuration. It will also be the testbed used for development of the wavefront sensor used for automatic, optimal alignment of the interferometer once lock has been achieved.

7. CONCLUSIONS

The LIGO project is intended to open the field of gravitational wave astrophysics by first providing experimental verification of gravita-

tional waves and then operating as a long term, extensible and adaptable observatory. The detection technique is to measure the strains induced in space by gravitational waves using laser interferometry between nearly free masses. The project is designed to permit phased incorporation, at later dates, of improvements in the technology of laser gravitational wave detection to further improve the instrumental sensitivity and bandwidth. The LIGO will be part of an international network of long baseline interferometric detectors to establish the polarization of the waves and the location of the astrophysical sources.

8. ACKNOWLEDGMENTS

I would like to acknowledge my colleagues on

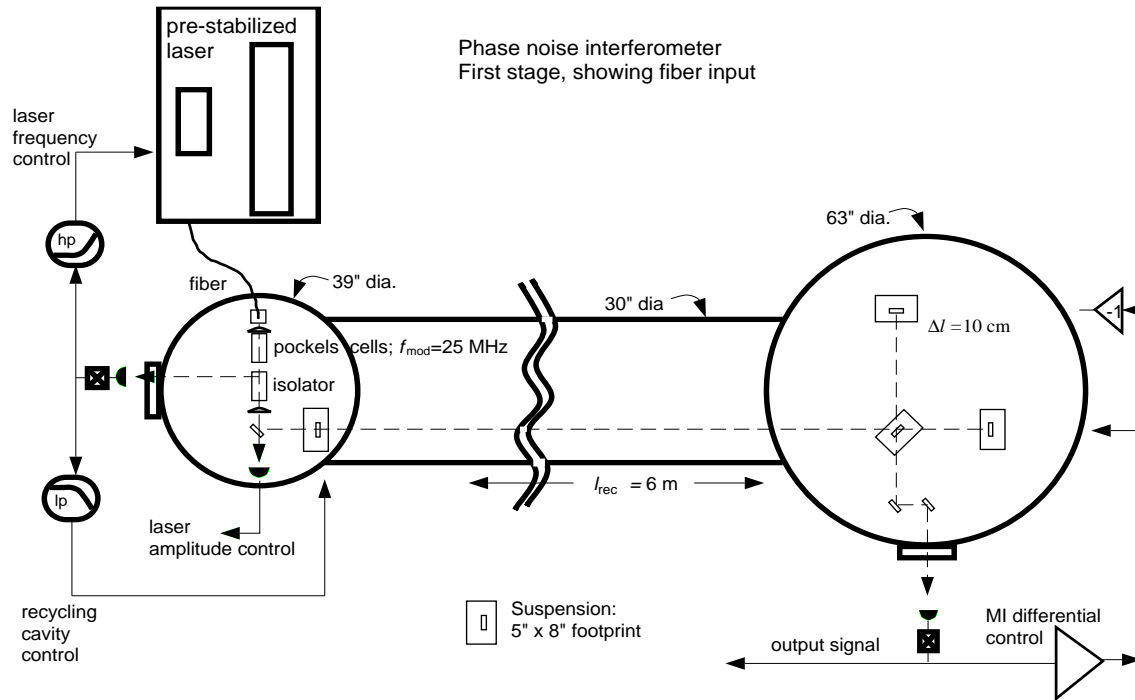


Figure 24: PNI initial configuration

the LIGO project, whose work has been reported here and who have been a source of encouragement and stimulation. I would also like to acknowledge the support of the National Science Foundation for LIGO, under cooperative agreement PHY-9210038.

9. REFERENCES AND NOTES

- [1] A. Abramovici, W. Althouse, R. Drever, Y. Gursel, S. Kawamura, F. Raab, D. Shoemaker, L. Seivers, R. Spero, K. Thorne, R. Vogt, R. Weiss, S. Whitcomb, M. Zucker, "LIGO: The Laser Interferometer Gravitational-Wave Observatory", *Science*, v256, 325-333, April 1992.
- [2] Misner, Thorne, Wheeler, *Gravitation*, N.Y.: W.H. Freeman & Co., 1973
- [3] B.F. Schutz, *A First Course in General Relativity*, Cambridge: Cambridge University Press, 1986
- [4] Hawking & Israel, Ed., *300 Years of Gravitation*, Cambridge: Cambridge University Press, 1990
- [5] P.R. Saulson, *Fundamentals of Interferometric Gravitational Wave Detectors*, New Jersey: World Scientific, 1994.
- [6] D.G. Blair, Ed., *The Detection of Gravitational Waves*, Cambridge: Cambridge University Press, 1991.
- [7] K.S. Thorne, *Gravitational Radiation: A New Window Onto the Universe*, Cambridge: Cambridge Univ. Press, 1989.
- [8] K.S. Thorne, in *300 Years of Gravitation*, S.W. Hawking and W. Israel, Eds., Cambridge: Cambridge Univ. Press, pp. 330-458, 1984.
- [9] B.F. Schutz, *Nature*, 323, 310, 1986.
- [10] H.D. Wahlquist, *Gen. Relativ. Gravit.*, 19, 1101, 1987.
- [11] C.W. Lincoln and C.M. Will, *Phys. Rev. D*, 42, 1123, 1990.
- [12] R. Drever, "Fabry-Perot cavity gravity-wave detectors", in *The Detection of Gravitational Waves*, ed. by D. Blair, Cambridge: Cambridge Univ. Press, 306-317, 1991.
- [13] B. Meers, "Recycling in laser-interferometric gravitational-wave detectors", *Phys. Rev. D*, 38, 2317-

2326, October 1988.

[14] J.A. Armstrong, *J. Opt. Soc. Am.*, 56, 1024, 1966.

[15] R. Weiss, "Electromagnetically Coupled Broadband Gravitational Antenna", *Q. Prog. Rep. Res. Lab. Electron. MIT* 105, 54-76, 1972.

[16] J. Giaime, Studies of Laser Interferometer Design and a Vibration Isolation System for Interferometric Gravitational Wave Detectors, PhD thesis, MIT, June 1995.

[17] C.N. Man, D. Shoemaker, M. Pham Tu and D. Dewey, "External Modulation Technique for Sensitive Interferometric Detection of Displacements", *Physics Letters A*, v148, n1,2, 8-16, August 1990.

[18] Y. Hefetz, N. Mavalvala, "Sensitivity of the LIGO interferometer to mirror misalignment and method for automatic alignment", presented at MG7, Stanford Univ., July 1994.

[19] R. Drever et. al., *Appl. Phys. B*, 31, 97, 1983.

[20] R. Forward, "Wideband laser-interferometer gravitational-radiation experiment", *Physical Review D*, 17, 2, 379-390, January 1978.

[21] J. Gea-Banacloche and G. Leuchs, "Squeezed states for interferometric gravitational-wave detectors", *J. Modern Optics*, v34, n6/7, 1987.

[22] F. Reif, *Fundamentals of Statistical and Thermal Physics*, New York: McGraw Hill, 1965.

[23] A. Gillespie and F. Rabb, "Thermal excited vibrations of the mirrors of laser interferometer gravitational-wave detectors", *Physical Review D*, 52, 2,, 577-585, July 1995.

[24] A. Gillespie and F. Rabb, "Thermal noise in the test mass suspensions of a laser interferometer gravitational-wave detector prototype", *Physics Letters A*, 178, 357-363, May 1993

[25] V. Braginsky, Moscow State University, unpublished communication and continuing research.

[26] K. Thorne, "Gravity gradient noise due to human motion near a test mass chamber", Caltech Report, LIGO-L950753-00-E, 21 September 1995.

[27] S. Whitcomb, "Optical pathlength fluctuations in

an interferometer due to residual gas", Technical Report, California Institute of Technology, October 1984.

and

R. Weiss, "Scattering by residual gas, Technical Report, Massachusetts Institute of Technology, February 1989.

[28] M. Zuker and S. Whitcomb, "Measurement of Optical Path Fluctuations due to Residual Gas in the LIGO 40 Meter Interferometer", presented at MG7, Stanford Univ., July 1994.

[29] C.M. Caves, *Physical Review D*, 23 1693, 1981.

[30] J. Giaime, P. Saha, D. Shoemaker, L. Seivers, "A passive vibration isolation stack for LIGO: design, modeling and testing", submitted to *Review of Scientific Instruments*, 31 May 1994.

[31] A. Abramovici, T. Lyons, F. Raab, "Measured limits to contamination of optical surfaces by elastomers in vacuum", *Applied Optics*, 34:1, 1 January 1995.

[32] G. Gonzalez and P. Fritschel, "Barry Controls STACIS isolators: performance in situ", Massachusetts Institute of Technology, LIGO-G952003-00-R, 26 May 1995.

[33] J. Camp, L. Sievers, R. Bork, J. Heefner, "Guided lock acquisition in a suspended Fabry-Perot cavity", submitted to *Optics Letters*, August 1995.

[34] A. Abramovici et. al., to be submitted to *Phys. Rev. D*, 1995.

[35] F. Raab, "Development of laser interferometer gravitational-wave detectors for LIGO", Proceedings of the OE/LASE: Lasers and Applications Conference (SPIE), January 1995.

10. BIOGRAPHY

Dennis Coyne is the Deputy Integration and Systems Engineering Manager for the LIGO Project at the California Institute of Technology. Prior to LIGO, he worked on adaptive optics, pointing and tracking and servo-control systems, as a principal scientist for Kaman Sciences Corporation, and on product design at Bell Labs. He has an MSME from the University of California at Berkeley and was a Commonwealth Scholar at the University of Massachusetts.